NASA TECHNICAL MEMORANDUM

NASA TM X-3064

NASA TM X-3064

CRUISE PERFORMANCE OF AN ISOLATED 1.15 PRESSURE RATIO TURBOFAN PROPULSION SYSTEM SIMULATOR AT MACH NUMBERS FROM 0.6 TO 0.85

by Fred W. Steffen

Lewis Research Center
Cleveland, Ohio 44135

NATIONAL AERONAUTICS AND SPACE ADMINISTRATION • WASHINGTON, D. C. • JUNE 1974

1. Report No.	2. Government Accession No.	3. Recipient's Catalog No.
NASA TM X-3064		

4. Title and Subtitle	5. Report Date
CRUISE PERFORMANCE OF AN ISOLATED 1.15 PRESSURE RATIO TURBOFAN PROPULSION SYSTEM SIMULATOR AT MACH NUMBERS FROM 0.6 TO 0.85	June 1974
	6. Performing Organization Code
7. Author(s)	8. Performing Organization Report No.
Fred W. Steffen	E-7824
	10. Work Unit No.
9. Performing Organization Name and Address	501-24
Lewis Research Center National Aeronautics and Space Administration Cleveland, Ohio 44135	11. Contract or Grant No.
	13. Type of Report and Period Covered
12. Sponsoring Agency Name and Address	Technical Memorandum
National Aeronautics and Space Administration Washington, D.C. 20546	14. Sponsoring Agency Code

15. Supplementary Notes

16. Abstract

An isolated 1.15 pressure ratio turbofan engine simulator was tested at Mach numbers from 0.6 to 0.85. At Mach 0.75 the net propulsive force of the fan and nacelle (excluding core thrust) was 73 percent of the ideal fan net thrust. Internal losses amounted to 7 percent, and external drag amounted to 20 percent of the ideal fan net thrust. External pressure and friction drag were about equal. The propulsive efficiency with a 90 percent efficient fan would have been 63 percent. For the aerodynamic characteristics of the nacelle that was tested, increasing the fan pressure ratio to approximately 1.35 would have resulted in a maximum propulsive efficiency of 67 percent.

17. Key Words (Suggested by Author(s))	18. Distribution Statement
Turbofan; Drag; Propulsive efficiency; STOL; Short haul aircraft; Simulator; Duct losses	Unclassified - unlimited Category 28

19. Security Classif. (of this report)	20. Security Classif. (of this page)	21. No. of Pages	22. Price*
Unclassified	Unclassified	50	$3.25

*For sale by the National Technical Information Service, Springfield, Virginia 22151

Page Intentionally Left Blank

CRUISE PERFORMANCE OF AN ISOLATED 1.15 PRESSURE RATIO TURBOFAN PROPULSION SYSTEM SIMULATOR AT MACH NUMBERS FROM 0.6 TO 0.85

by Fred W. Steffen

Lewis Research Center

SUMMARY

An isolated 1.15 pressure ratio turbofan engine simulator was tested at Mach numbers from 0.6 to 0.85. Values of nacelle thrust minus drag, propulsive efficiency, inlet and nozzle performance, and component pressure distributions were obtained.

At Mach 0.75 the propulsive force of the nacelle (excluding core thrust) was 73 percent of the ideal fan net thrust. Internal losses amounted to 7 percent of the ideal fan net thrust, and external drag amounted to 20 percent of the ideal fan net thrust. For this condition the external pressure drag was approximately equal to calculated friction drag level. At Mach 0.75 the propulsive efficiency with a 90 percent efficient fan would have been 63 percent. For the aerodynamic characteristics of the nacelle that was tested, a fan pressure ratio of 1.35 would have resulted in a propulsive efficiency of 67 percent. With the fan feathered, the total force coefficients were about twice the external drag coefficients with power on.

INTRODUCTION

The use of a low-pressure-ratio turbofan propulsion system for an externally blown flap short haul aircraft is of interest because of its potentially low fan and flap impingement noise levels and its potentially high propulsive efficiency. Low pressure ratios may also permit the use of variable pitch fans which offer the potential of lightweight thrust reversal systems, improved thrust response, and minimized fan exit area variations. For commercial applications, the noise characteristics of such a fan may reduce the amount of acoustic wall treatment required in the fan duct and may eliminate the need for acoustic splitters.

For a given level of thrust, however, the fan and nacelle would be larger than those

of a higher pressure ratio system. Thus, the nacelle drag at cruise speeds could be a higher percentage of the net thrust. Also, since there would be only a small increase in exit velocity above the free stream value, small losses in the fan duct could result in large losses in net thrust.

The performance of some low-pressure-ratio fixed pitch fans is reported in references 1 and 2. The potential of variable pitch fan systems is discussed in references 3 and 4. Because of the current interest in propulsion systems for low noise, short haul aircraft, an experimental investigation was undertaken to study the performance characteristics of an isolated 1.15-pressure-ratio variable pitch fan system over the entire operating range of a short haul transport. A fan pressure ratio of 1.15 was chosen as the lowest value likely to be of interest and the most sensitive to potential losses. The 50.8 centimeter (20 in.) diameter fan was installed in a nacelle designed for a cruise Mach number of 0.75. The fan was driven by an air turbine within the core of the nacelle. The core size, relative to the fan diameter, was representative of a 25:1 bypass ratio engine. Three inlet configurations, differing in internal lines (contraction ratio) and overall lengths, were evaluated. This report presents the cruise performance of the nacelle with these inlets. The low speed performance is presented in reference 5, and a summary of the low and high speed performance is presented in reference 6.

Cruise tests were conducted in the Lewis Research Center 8- by 6-Foot Supersonic Wind Tunnel at zero angle of attack for Mach numbers from 0.6 to 0.85 and Reynolds number per meter from 12.3×10^6 to 14.3×10^6. At each Mach number the fan was run over a range of speeds to vary pressure ratio and flow rate. Overall nacelle thrust minus drag, propulsive efficiency, drag data, inlet and nozzle performance, and component pressure distributions are presented.

APPARATUS AND PROCEDURE

Nacelle Design

Photographs of the simulator nacelle installed in the 8- by 6-Foot Supersonic Wind Tunnel are presented in figure 1. A cross-sectional view of the nacelle is shown in figure 2. The symbols used in the figure, as well as all other symbols, are defined in appendix A. The fan used in the nacelle was a single-stage axial flow design with a tip solidity of 0.5. The fan had 12 adjustable pitch rotor blades and 32 stator blades. It had a hub to tip ratio of 0.4. To minimize fan noise the rotor and stator were separated by three chord lengths.

The fan was driven by a four-stage turbine within the core of the nacelle. Turbine drive air came from a 3.103×10^6 newtons per square meter (450 psi) continious flow supply system, and it was heated to a temperature of 366 K (660° R). The turbine per-

formance is described in reference 7.

The overall dimensions of the nacelle are shown in figure 2. The fan was tightly wrapped with an axisymmetric cowl to minimize surface and cross-sectional area; this design resulted in a D_{FT}/D_{MAX} of 0.93. The surface area of the fan cowling was, of course, influenced by the rotor-stator spacing and could have been reduced if a smaller rotor-stator spacing had been chosen. The core had no air inlets but the dimensions were otherwise typical of an actual gas turbine drive system for a 25:1 bypass ratio engine.

The nacelle was supported by a dorsal fin and pylon, the latter having a thickness to chord ratio of 11.25 percent. The pylon coordinates are presented in table I. The pylon was supported from flexure plates within a windshield. A load cell was used to measure the thrust-minus-drag forces on the nacelle, dorsal, and pylon.

Inlet Design

The inlet geometries that were investigated are summarized in figure 3. Three inlet-spinner combinations were used for these cruise tests and are referred to as 1-1, 2-2, and 2-1. The first digit designates the outer cowling and the second digit designates the spinner. Cowling 1 differed from cowling 2 primarily in contraction ratio A_1/A_T; it was 1.26 for cowling 1 and 1.35 for cowling 2. Both cowls had the same maximum diffuser wall angles. Thus, cowl 2, with a higher contraction ratio, had a longer diffuser and external cylindrical section than cowl 1. Both cowls had the same NACA 1 series external contours obtained from reference 8. An inlet diameter ratio D_1/D_{MAX} of 0.935 and a forebody length ratio X_{FF}/D_{MAX} of 0.175 were used for both cowls. These values were obtained from the drag divergence correlation of reference 9 for a drag divergence Mach number of 0.8 at a mass flow ratio $W_F/W_{0,MAX}$ of 0.65.

The spinners differed in length such that the nose of spinner 1 was tangent to the throat plane of cowl 1 and the nose of spinner 2 was tangent to the throat plane of cowl 2.

Nozzle Design

The fan nozzles that were investigated are shown in figure 4. Nozzle 1 is the cruise nozzle and was sized to give an inlet mass flow ratio of approximately 0.65 at a free stream Mach number of 0.75 with a fan pressure ratio of 1.15. The nozzle had a terminal boattail angle of 16° and a boattail juncture radius to maximum diameter ratio of 0.93. At Mach 0.75, with a fan pressure ratio of 1.15, the nozzle pressure ratio was 1.66. Fan nozzle 2 had a larger area than 1 and was used to obtain inlet drag data at high mass flow ratios and nacelle force data with the fan feathered.

The core nozzle, shown in figure 5, had internal lines which formed a constant area

duct. The core boattail was contoured essentially the same as the fan nozzle boattail. However, it had a projected boattail area of only 3.9 percent of the nacelle maxium cross-sectional area compared to 21.8 percent for fan nozzle 1. The core boattail was scrubbed by the fan jet which had a flow Mach number of about 0.9 at the design cruise condition.

Test Procedure

For a tunnel Mach number of 0.6, data were recorded at fan mechanical speeds from 8500 to 12 000 rpm in 500 rpm increments. Data were recorded at these same mechanical speeds at Mach 0.7, 0.75, 0.80, and 0.85 and repeated at Mach 0.75.

All reported data were taken at a zero angle of attack. Reynolds number per meter varied from 12.3×10^6 at Mach 0.6 to 14.3×10^6 at Mach 0.85.

Instrumentation and Data Reduction

The pressure and temperature instrumentation installed in the nacelle is shown in figure 6. The fan inlet pressure P_2 was obtained from an area weighted average of the pressures measured with three outer wall boundary layer rakes and free stream total pressure, which was assumed to exist over the rest of the annulus. This assumption was made because inner wall (spinner) boundary layer losses were expected to be small at normal operating flow rates. At choked inlet conditions, however, P_2 could not be accurately determined with this instrumentation. Thus, data which depend on P_2 are not presented at these conditions.

Fan outlet pressure P_3 was obtained from a mass weighted average of 18 pressures measured on three rakes at station 3. For mass weighting, a constant total temperature was assumed to exist throughout the annulus along with a linear static pressure gradient from inner wall to outer wall. Inner wall boundary layer rakes were also located at station 3 but were used only to define nozzle inlet pressure profiles.

Turbine inlet pressure and temperature were obtained from an average of two pressures and two temperatures. Turbine outlet pressure and temperature were obtained from area weighted averages of six total pressures and six total temperatures obtained with four rakes. Turbine weight flow was measured with a standard ASME sharp edged orifice.

All pressure drags were obtained from area weighted averages of surface static pressures - three rows on the fan boattail, three rows on the core boattail, one row on the external pylon, and one row on the scrubbed pylon. For the external pylon pressure drag, the pressure distribution measured with the upper row of pylon static pressure taps was assumed to exist over the entire pylon and dorsal down to a fan jet boundary line

extending aft in an axial direction from the fan nozzle tip. For the scrubbed pylon pressure drag, the pressure distribution measured with the lower row of pylon taps was assumed to exist over the region aft of the fan exit plane and below the fan jet boundary line.

Corrected fan weight flow was obtained by relating corrected weight flow to the pressure ratio (p/H_0) obtained from one or more static taps in the inlet. To establish this relation, an experimental internal pressure ratio distribution, for which the corrected weight flow was unknown, was compared to a series of theoretical pressure distributions for which the corrected weight flows were known. The theoretical pressure ratio distributions were obtained from an axisymmetric potential flow analysis using corrected weight flow as an input. Such a comparison is shown in figure 7 for Mach 0.75. Additional comparisons were made at other fan operating conditions and other free stream Mach numbers.

On the basis of these comparisons a region near the throat was selected. In this region the trends of the theory and the experimental data were in good agreement, boundary layer effects were negligible, and the wall pressure was the most sensitive to weight flow variations. The region near the fan was rejected because of the uncertain effects associated with boundary layer growth and radial static pressure gradients caused by the fan and unaccounted for in the theory. The region near the highlight was also rejected because of the insensitivity of the pressure to weight flow variations.

Theoretical pressure ratios in the selected throat region, or more specifically values at points a and b (see fig. 7), were tabulated against corrected weight flow and are presented in tables II, III, and IV for a range of free stream Mach numbers. The experimental corrected weight flow was obtained from an average of the two corrected weight flows obtained from the tables for the experimental pressure ratios measured at points a and b. For example, for the data in figure 7 a corrected weight flow of 78.07 (times the reference value) was determined to be the correct experimental value.

The same axisymmetric potential flow analysis also provided values of additive drag coefficient and stagnation point radius ratio R_{STAG}/R_1 for each corrected weight flow and free stream Mach number. These are presented in table I for inlet 1-1. However, inspection of the variation of corrected weight flow with the pressures measured by several static pressure taps near the stagnation point showed that the experimental stagnation point location did not quite agree with the theoretical location. The experimental and theoretical stagnation point locations are compared in figure 8. To obtain an axisymmetric potential flow additive drag using the experimental stagnation point location, a one-dimensional additive drag was computed using the experimental stagnation station and corrected weight flow. The value was then multiplied by the ratio of axisymmetric potential flow additive drag to one-dimensional additive drag for the same corrected flow rate (but with the potential flow stagnation point). In this manner the axisymetric potential flow additive drag, using the experimental stagnation station, was obtained.

The cowl suction force was obtained from an area weighted average of three rows of cowl static pressures extending from the experimental stagnation point to the maximum diameter of the nacelle. The difference between axisymmetric potential flow additive drag (computed using the experimental stagnation point) and cowl suction force is defined as the inlet pressure drag. Inlet pressure drags for inlets 2-2 and 2-1 are not presented because severe pressure gradients at and just inside the inlet highlight made it impossible to accurately calculate the cowl suction force with the available instrumentation. The equations used to obtain the other performance parameters in this report are contained in appendix B.

RESULTS AND DISCUSSION

Overall Performance

As mentioned previously, three different inlets were tested on the nacelle. These inlets differed in internal lines and length and were not expected to give large differences in cruise performance. A comparison of nacelle thrust minus drag against free stream Mach number with the three different inlets is shown in figure 9 for two values of fan pressure ratio. At a fan pressure ratio of approximately 1.1, where the fan flow rates were low, no differences in propulsive force were noted across the Mach number range. However, at a fan pressure ratio of approximately 1.15, where the fan flow rates were high, inlet 2-2 with the 1.35 contraction ratio cowl and the long spinner gave a somewhat lower performance over the Mach number range. The performance loss probably was caused by inlet losses associated with high inlet internal velocities. At Mach 0.75 and above the flow in the inlet actually choked. Thus, inlet 2-2 was not acceptable for cruising flight. Use of the short spinner with the 1.35 contraction ratio cowl, inlet 2-1, alleviated choking and resulted in an acceptable inlet.

Since inlets 2-1 and 1-1 had the same performance characteristics, as indicated in figure 9, data taken with inlet 1-1 are considered to be representative of either inlet and are used in all of the remaining figures. Also, data taken with the fan pressure ratio closest to 1.15 were selected for presentation in most of the remaining figures. The mass flow ratio Mach number schedule that resulted from this selection is presented in figure 10. The mass flow ratio varied from 0.700 at Mach 0.6 to 0.645 at Mach 0.85. These mass flow ratios were slightly higher than design values because the fan nozzle had a slightly larger effective area than anticipated.

The overall measured performance of the nacelle is represented by the bottom curve in figure 11. This curve is the nacelle net propulsive force (or load cell force) less core thrust divided by the ideal fan net thrust. The ideal fan net thrust is the net thrust calculated from the fan pressure ratio and weight flow with no internal losses. A breakdown

of the loss in net thrust from the ideal value is also presented in figure 11. The measured pressure drag and the calculated flat plate friction drag were added to the bottom curve to obtain the two intermediate curves. The top curve was obtained by calculating a net thrust based on a measured fan outlet pressure, which for a particular fan pressure ratio reflected the inlet loss. The difference between the two top curves was considered to be the nozzle internal loss.

At Mach 0.75 only 73 percent of the ideal fan net thrust was available for propulsion. The inlet internal loss accounted for about 2 percent of ideal fan net thrust and the nozzle internal loss an additional 5 percent; this condition resulted in a total internal loss of 7 percent. The calculated flat plate friction drag accounted for a 10 percent loss of fan net thrust, and the measured pressure drag also accounted for a 10 percent loss. The total drag of the nacelle and pylon represented a loss of 20 percent of ideal fan net thrust. The rapid decrease in overall performance above Mach 0.8 was due to inlet drag rise.

At Mach 0.6 the approach just described lead to a negative nozzle loss or, in terms of nozzle performance, a gross thrust efficiency of 1.003. As explained in appendix C, a small part of the efficiency over 1.000 can be theoretically accounted for by the fact that the nozzle is unchoked and the pressure at the exit plane exceeds p_0. For the most part, however, the excess in gross thrust efficiency is probably due to inaccuracies in determining the component drags, core thrust, fan nozzle inlet pressure, and fan weight flow.

Drag coefficients for the nacelle and pylon are shown in figure 12 for the nominal fan pressure ratio and mass flow ratio schedule. A drag coefficient line equal to 25 percent of ideal fan net thrust is included for reference. At Mach 0.75 the drag coefficient for the combined nacelle, dorsal, and pylon was approximately 0.052. Flat plate friction drag was about half of the total drag; in other words, friction drag and pressure drag were about equal for this nacelle, dorsal, and pylon. Above Mach 0.75 the pressure drag increased rapidly due to divergence of the inlet cowl drag.

At Mach 0.75 an estimation of friction drag was made using the velocities calculated from pressures measured experimentally on the fan cowl. These supervelocities slightly increased the friction drag above flat plate values as indicated in figure 12.

In figure 13 the propulsive efficiency of the nacelle is shown as a function of free stream Mach number. Because the efficiency of the experimental fan used in the simulator was not typical of the efficiency that might be obtained from a highly developed fan, assumed values of fan efficiency were used. At Mach 0.75 the propulsive efficiency with a 100 percent efficient fan was 70 percent. With a more realistic value for fan efficiency of 90 percent, the propulsive efficiency dropped to 63 percent.

For high propulsive efficiency the nacelle should be designed to handle as large a corrected weight flow per unit of nacelle cross-sectional area (specific corrected flow) as possible. Figure 14 shows the effect of specific corrected flow on analytical propul-

sive efficiency over a range of fan pressure ratios for two values of drag coefficient. Specific corrected flow values of 0.0147 kilogram per second per square centimeter (value for the nacelle and fan of this report) and 0.0104 kilogram per second per square centimeter (typical value for a lower bypass ratio fan-nacelle system) were selected. A fan efficiency of 0.90 has been assumed and the effects of the core thrust and internal inlet and exhaust duct losses have been neglected. The effect of high specific corrected flow is most important at low fan pressure ratios and high nacelle drag coefficients. The high experimental value of specific corrected flow was achieved by using a thin walled nacelle ($D_{FT}/D_{MAX} = 0.930$), fan rotor blade setting that gave a fan face Mach number of 0.6, and a fan design which had a hub to tip ratio of only 0.4. Figure 14 also shows that for a nacelle drag coefficient of 0.06 (near the measured value of 0.052 for the test nacelle) the fan pressure ratio for maximum efficiency should be about 1.35 for the high specific corrected flow rate and about 1.45 for the low specific corrected flow rate. The corresponding propulsive efficiencies would be 0.665 and 0.630, respectively.

Component Pressure Drags

Component pressure drags are shown in figure 15. A drag coefficient line equal to 5 percent of ideal fan net thrust is included for reference. Experimental values are shown over the Mach number range, and an estimated value is shown at Mach 0.75.

In figure 15(a) the inlet pressure drag from Mach 0.6 to Mach 0.75 was slightly negative and considerably below the value obtained from reference 10. Results of potential flow calculations, which will be discussed later, indicate that the level may be influenced by the pressure field from the boattail acting on the inlet. Drag rise occurred at approximately the design drag divergence Mach number of 0.8, as estimated from reference 9 for this high diameter ratio, short inlet.

In figure 15(b) the fan boattail pressure drag coefficient is shown. This was the largest component of pressure drag at Mach 0.75. Its value was somewhat higher than the estimated value from reference 11, even though the ratio of boattail projected area to maximum cross-sectional area was less for the fan boattail than for the boattail of reference 11 (0.220 as opposed to 0.492). Above Mach 0.75 the boattail pressure drag coefficient decreased slightly as the inlet pressure drag increased rapidly. These results again imply a possible interaction between the inlet and fan nozzle boattail.

The core boattail pressure drag coefficient is shown in figure 15(c). At Mach 0.75 the measured value agreed with the estimated value obtained from reference 11. Above Mach 0.7 the measured value increased with increasing Mach number. It should be noted that the drag coefficient in figure 15(c) was based on q_0 and A_{MAX}. If based on local q and centerbody cross-sectional area, the value for the core boattail at Mach 0.75 would have been about 0.03.

Both the scrubbed (fig. 15(d)) and the external (fig. 15(e)) pylon pressure drag coefficients were considerably higher than the very low levels of pressure drag estimated from the airfoil method of reference 12. Together they accounted for a drag of about 5 percent of the ideal fan net thrust. As indicated by the pressure distributions in appendix C, some of the pylon drag resulted from failure of the flow to fully recompress on the rather abrupt closure of the pylon afterbody. Hopefully, much of the drag could be eliminated in a redesigned pylon.

A potential flow analysis was used to determine the effect of boattail proximity in inlet pressure drag. The experimental values of inlet drag coefficient and inlet-boattail proximity were used as reference values. Additive drag was held constant (as indicated by the analysis to be a valid assumption) and increments of cowl suction force were determined. The results are shown in figure 16. As the boattail was moved closer to the inlet, inlet cowl suction was increased and thus inlet pressure drag was reduced. This result and the experimental trends of figure 15 show that an interaction exists between the inlet cowl and fan boattail for this type of geometry. This makes it highly desirable to test the fan inlet and nozzle simultaniously.

The variation of inlet pressure drag coefficient with mass flow ratio is shown in figure 17. To extend the range of mass flow ratios, data obtained with nozzles 1 and 2 are shown. This change in nozzle geometry appears to have had a negligible effect on inlet drag as evidenced by a small and random change in the drag coefficient level where the two sets of data overlap. For Mach numbers up to 0.80 (figs. 17(a) to (d)) the drag coefficients appraoched a minimum value of less than zero as the mass flow ratio was increased. At Mach 0.85 (fig. 17(e)) the inlet choked before a minimum value was reached.

The additive drag and cowl suction coefficients (which are algebraically summed to obtain the inlet pressure drag coefficient) are shown in figure 18 as functions of the mass flow ratio. Data for Mach 0.75 and 0.85 are presented. At all the mass flow ratios presented, the additive drag coefficient was somewhat higher at Mach 0.85 than at Mach 0.75, and the cowl suction coefficient was considerably less at Mach 0.85 than at Mach 0.75. At Mach 0.75 the cowl suction coefficient exceeded the additive drag coefficient at mass flow ratios greater than 0.64. At Mach 0.85 the cowl suction coefficient was considerably below the additive drag coefficient at any of the mass flow ratios shown.

A further explanation of the reduction in cowl suction force as the Mach number is increased from 0.75 to 0.85 is obtained by examining the cowl pressure distributions. Cowl pressure coefficients at Mach 0.75 and 0.85, for a mass flow ratio of 0.658, are plotted against projected area ratio in figure 19. The cowl suction coefficient is the difference between the cross-hatched areas above and below the curve. The stagnation and highlight pressure coefficients are less at Mach 0.75 than at Mach 0.85, and thus the area under the curve (labeled drag) is less at Mach 0.75 than at Mach 0.85. Also, the minimum pressure coefficients are lower at Mach 0.75 than at Mach 0.85, and thus

the area above the curve (labeled thrust) was slightly greater at Mach 0.75 than at Mach 0.85. This was true even though the pressure coefficients at Mach 0.85 remained nearly constant at the maximum negative value, indicating a possible separation of flow from the cowl. These distributions were typical for the entire range of mass flow ratios tested at Mach 0.75 and 0.85. Additional pressure distributions on the fan cowl and other nacelle components at the nominal fan pressure ratio and mass flow ratio schedule are presented in appendix D.

Fan boattail pressure drag coefficients obtained from pressure integrations are shown as a function of fan nozzle pressure ratio in figure 20. At all free stream Mach numbers the drag coefficient decreased slightly with increasing nozzle pressure ratio, although the range of nozzle pressure ratios at each Mach number was quite limited. The drag coefficient also decreased with increasing Mach number, but the decrease is probably due to the increasing pressure ratio that accompanied the increase in Mach number. These results do not agree with the results shown in reference 11 where an increase in boattail drag was noted when the nozzle pressure ratio increased from 1.5 to 2.0 at a constant Mach number of 0.85. The disagreement may result from differences in forebody geometry. The data in reference 11 were obtained with a long cylinderical forebody as opposed to the data of this report which were obtained with a short forebody.

Forebody effects were seen in the boattail pressure distributions. Unlike the pressure distributions in reference 11, the fan boattail pressure distributions (appendix D) did not, in general, exhibit a sharp drop in pressure near the boattail juncture but instead began at about the level of the last inlet cowl pressure and increased continuously to the level at the exit plane.

Core boattail pressure drag coefficients obtained from pressure integrations are shown as a function of core nozzle pressure ratio in figure 21. Fan nozzle pressure ratios, which determine the flow conditions over the core boattail, are indicated. At free stream Mach numbers of 0.75 and below, the boattail drag coefficient was invariant with core nozzle pressure ratio or free stream Mach number. Above Mach 0.75 the core boattail drag coefficient increased with increasing core nozzle pressure ratio and increasing free stream Mach number. The core boattail pressure distributions are also presented in appendix D.

Fan Nozzle Coefficients

The fan nozzle flow coefficients are presented in figure 22, and the fan nozzle gross thrust efficiencies are presented in figure 23. The methods for obtaining these coefficients are explained in appendix B. In general, the flow coefficients increased with both fan nozzle pressure ratio and free stream Mach number. At design conditions the fan

nozzle flow coefficient was about 0.95. The gross thrust efficiencies were, in general, independent of pressure ratio at each Mach number and decreased with increasing Mach number. At design conditions the fan nozzle gross thrust efficiency was 0.995. At Mach 0.6 the gross thrust efficiency was about 1.003 (see appendix C). These results are not unique for the fan nozzle geometry but depend on the pressure profiles at the entrance to the fan nozzle, and, since the nozzle was unchoked, on the pressure surrounding the nozzle exit plane. The pressure profiles at the nozzle entrance and the fan boattail pressures are presented in appendix D. The boattail pressure distributions indicate that the pressure surrounding the nozzle exit was above ambient.

Feathered Performance

Low-pressure-ratio fans of the type used in this nacelle are often considered to be variable pitch devices. Thus, if the core engine becomes inoperative, the fan could be feathered and the drag of the engine and nacelle somewhat reduced. To determine the drag level under these conditions the adjustable pitch blades of the model fan were set at an estimated angle for feather and the larger fan nozzle installed. Since the estimated blade angle for feather was slightly in error, the fan rotated counterclockwise (as opposed to its normal clockwise rotation) at speeds from 870 to 970 rpm. The force coefficients obtained with this configuration are presented in figure 24. They amounted to about twice the drag coefficient measured during power on operation. This would be expected as the total wetted area is about doubled when the fan duct internal flow surfaces are accounted for. Drag rise appeared to occur at a Mach number slightly above 0.7.

SUMMARY OF RESULTS

An isolated 1.15 pressure ratio turbofan engine simulator was evaluated at Mach numbers from 0.6 to 0.85. Values of nacelle thrust minus drag, propulsive efficiency, drag, inlet and nozzle performance, and component pressure distributions were obtained.

At Mach 0.75 the net propulsive force of the nacelle (excluding core thrust) was 73 percent of the inlet fan net thrust. Internal losses amounted to 7 percent and drag amounted to 20 percent of the ideal fan net thrust. For this nacelle, friction and pressure drag were about equal with fan boattail pressure drag being the largest component of pressure drag. At Mach 0.75 the drag coefficient for the nacelle, dorsal, and pylon was about 0.052. Drag divergence occurred at the inlet design value of 0.8.

For Mach numbers up to 0.80 the inlet pressure drag coefficient approached a minimum value of less than zero as mass flow ratio was increased. A potential flow analysis showed that inlet pressure drag could be a function of the fan boattail proximity. The

fan boattail pressure drag coefficient in general decreased with increasing fan nozzle pressure ratio and free stream Mach number. Fan boattail pressure distributions appeared to be influenced by the close proximity of the inlet.

At Mach 0.75 the propulsive efficiency, assuming a 90 percent efficient fan and excluding core thrust, would have been 63 percent. An analysis showed that for a drag coefficient of 0.06 and the high corrected weight flow per unit area attained with the simulator, a fan pressure ratio of about 1.35 would be necessary to obtain a maximum propulsive efficiency of 67 percent.

Fan nozzle flow coefficient increased with both fan nozzle pressure ratio and free stream Mach number. At design conditions the fan nozzle flow coefficient was 0.95. Fan nozzle gross thrust efficiency was independent of pressure ratio at each Mach number and decreased with increasing Mach number. At design conditions the fan nozzle gross thrust efficiency was 0.995. An analysis showed that the fan nozzle, which operated unchoked and discharged into a flow field where the static pressure was above ambient, could theoretically have had a gross thrust efficiency greater than 1.000.

Lewis Research Center,
National Aeronautics and Space Administration,
Cleveland, Ohio, February 25, 1974,
501-24.

APPENDIX A

SYMBOLS

A	area
C_D	drag coefficient, $D/q_0 A_{MAX}$
C_p	pressure coefficient, $p - p_0/q_0$
c	chord
c_p	specific heat of air at constant pressure
D	diameter or drag
D_f	friction drag
F_{LOAD}	force measured by load cell
F_{CORE}	calculated gross thrust of core stream, $\frac{0.9830\ W_{CORE}\ V_{ICORE}}{g}$
F_{GFi}	gross thrust of fan stream obtained by isentropic expansion of fan flow from P_3 and T_3 to p_0
F_{GFi}'	gross thrust of fan stream obtained by isentropic expansion of fan flow from P_3' and T_3 to p_0
F_{NFI}	net thrust of fan stream with only internal inlet losses and no nozzle losses
F_{NFII}	net thrust of fan stream with both internal inlet and nozzle losses
F_{NFIII}	net thrust of fan stream with all internal losses and external friction drag
F_{NFIV}	net thrust of fan stream with all internal losses and external friction and pressure drag
F_{NFi}	ideal net thrust of fan stream
g	gravitational constant
K	mechanical equivalent of heat
M	Mach number
P	total pressure
P_3'	ideal total pressure at fan exit

p	static pressure
q	dynamic pressure
R	radius or gas constant
Re	Reynolds number
T	total temperature
t	thickness
V	velocity
V_I	ideal velocity obtained by isentropic expansion of flow from nozzle inlet pressure and temperature to ambient pressure
V_{ICORE}	ideal velocity of core flow obtained by isentropic expansion of core flow from P_5 and T_5 to p_0
W_F	fan flow rate, calculated at inlet
W_{Fi}	ideal fan flow rate
$W_{0,MAX}$	free stream flow rate through a stream tube with cross-sectional area A_{MAX}
x	length
β	boattail angle
γ	ratio of specific heats
σ	effective full cone angle of diffuser from A_{MIN} to A_2
η_G	fan nozzle gross thrust efficiency
η_{GA}	analytical gross thrust efficiency
η_P	propulsive efficiency
η_{PA}	analytical propulsive efficiency
φ	maximum turning angle of diffuser
ψ	angular coordinate, measured counterclockwise from bottom looking aft

Subscripts:

a, b	inlet weight flow stations
ADD	additive
CB	core centerbody

CE	core exit
$C\beta$	core boattail
D	diffuser or drag
DD	drag divergence
e	annular exit area
F	fan
FC	fan cowl
FE	fan exit
FF	length of external contour of inlet
FH	fan hub
FT	fan tip
$F\beta$	fan boattail
I	inlet
L	local
M	length from inlet highlight to end of diffuser
MAX	maximum diameter or cross-sectional area of nacelle
MIN	minimum annular flow area in diffuser measured normal to axis
OA	overall
p	pressure
PROJ	projected
S	spinner
STAG	stagnation
STD	standard
T	throat
0	free stream conditions
1	highlight station
2	fan inlet station
3	fan exit station
4	turbine inlet station
5	turbine exit station

APPENDIX B

CALCULATION OF FRICTION DRAG, NET THRUST, GROSS THRUST EFFICIENCY, AND PROPULSIVE EFFICIENCY

Friction drag was calculated from

$$D_f = \frac{0.074(1 - 0.12\,M^2)qAw}{\left(x\frac{Re}{x}\right)^{1/5}}$$

Appropriate values of each of the variables were used for each component of the nacelle. The characteristic lengths and wetted areas are listed in table V.

The net thrust of the fan stream with only internal inlet losses and no nozzle losses was calculated as

$$F_{NFI} = F_{GFi} - \frac{W_F V_0}{g}$$

where F_{GFi} is the gross thrust obtained by isentropically expanding the fan flow W_F from measured P_3 and T_3 to p_0. The W_F was obtained by the procedure described in the Instrumentation and Data Reduction section.

The net thrust of the fan stream with both inlet and nozzle internal losses was obtained by adding all drag forces to the load cell force and substracting a calculated core thrust:

$$F_{NFII} = F_{LOAD} + \sum D_p + \sum D_f - F_{CORE}$$

The equation used to obtain the net thrust of the fan stream with all internal losses and external friction drag was

$$F_{NFIII} = F_{LOAD} + \sum D_p - F_{CORE}$$

The equation used to obtain the net thrust of the free stream with all internal losses and all external drag was simply

$$F_{NFIV} = F_{LOAD} - F_{CORE}$$

The ideal net thrust of the fan stream is defined as

$$F_{NFi} = F_{GFi}' - \frac{W_F V_0}{g}$$

where F_{GFi}' is the gross thrust obtained by expanding the fan flow from the ideal fan outlet pressure, P_3', and T_3 to p_0. The ideal fan outlet pressure is defined as

$$P_3' = \left(\frac{P_3}{P_2}\right) P_0$$

Using the measured fan outlet temperature T_3 instead of an ideal fan outlet temperature had a negligible effect on the results.

Propulsive efficiency (see fig. 13) is obtained from

$$\eta_p = \frac{(F_{LOAD} - F_{CORE})V_0}{\text{Power to fan}}$$

where

$$\text{Power to fan} = \frac{K}{\eta_F} W_F c_p T_0 \left[\left(\frac{P_3}{P_2}\right)^{(\gamma-1)/\gamma} - 1\right]$$

Analytical propulsive efficiency (see fig. 14) is obtained from

$$\eta_{PA} = \frac{\eta_F M_0 \sqrt{\gamma g R}}{Kc_p \left[\left(\frac{P_3}{P_2}\right)^{(\gamma-1)/\gamma} - 1\right] \left(1 + \frac{\gamma - 1}{2} M_0\right)^{1/2}} \left\{ \sqrt{\frac{\gamma R}{g}} \left(\frac{P_3}{P_2}\right)^{(\gamma-1)/2\gamma} \right.$$

$$\times \frac{M_e}{\left(1 + \frac{\gamma - 1}{2} M_e^2\right)^{1/2}} - \frac{M_0}{\left(1 + \frac{\gamma - 1}{2} M_0^2\right)^{1/2}} - \frac{\gamma}{2} \frac{C_D M_0^2}{\frac{\omega \sqrt{\varphi_2}}{\delta_2 A_{MAX}} \frac{\sqrt{T_{STD}}}{P_{STD}}}$$

$$\left. \times \frac{1}{\left(1 + \frac{\gamma - 1}{2} M_0^2\right)^{\gamma/(\gamma-1)}} \right\}$$

Ideal fan weight flow (see fig. 22) is obtained from

$$W_{Fi} = \frac{\sqrt{\frac{\gamma g}{R}} \left\{ \frac{2}{\gamma - 1} \left[\left(\frac{P_3}{p_0} \right)^{(\gamma-1)/\gamma} - 1 \right] \right\}^{1/2} P_3 A_e}{\left(\frac{P_3}{p_0} \right)^{3(\gamma-1)/\gamma} \sqrt{T_3}}$$

Fan nozzle flow coefficient was defined as W_F/W_{Fi}. Fan nozzle gross thrust efficiency (ref. fig. 23) was obtained from

$$\eta_g = \frac{F_{NFII} + \frac{W_F V_0}{g}}{F_{GFi}}$$

APPENDIX C

ANALYTICAL GROSS THRUST EFFICIENCY

Analytical gross thrust efficiency is defined as

$$\eta_{GA} = \frac{\frac{W_F V_e}{g} + A_e(p_e - p_0)}{\frac{W_F}{g} V_I} \tag{C1}$$

where the subscript e refers to the exit plane, subscript 0 refers to ambient conditions, and V_I is the velocity obtained by an isentropic expansion of the fan flow from the nozzle inlet pressure P_3 and temperature T_3 to p_0. For exit plane velocities less than sonic, the flow would appear as in sketch (a) for $p_e/p_0 > 1.0$ and as in sketch (b)

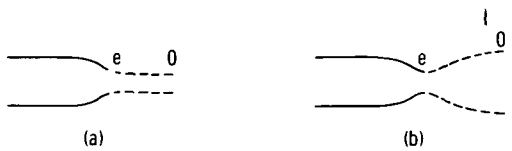

for $p_e/p_0 < 1.0$. For both cases the pressure acting on the stream tube downstream of the exit plane reduces the momentum of the stream from its value at the exit. Since the actual thrust is based on the momentum at the exit plane and the ideal thrust is based on the momentum of the stream expanded to p_0, the gross thrust efficiency for these operating conditions would be greater than 1.0. If the nozzle and boattail walls had been extended to a region of p_0, the pressure which reduced the momentum of the air in the previous examples would now reduce the boattail drag. Conversely, the shorter boattails shown in sketches (a) and (b) have more boattail drag than if they had been extended to a region of p_0.

For air, $\gamma = 1.4$, and unchoked flow, the equation for analytical gross thrust efficiency reduces to

$$\eta_{GA} = \frac{7.00098\sqrt{\left(\frac{p_e}{P_3}\right)^{1.42855}\left[1 - \left(\frac{p_e}{P_3}\right)^{0.28571}\right]^2} + \frac{p_0}{P_3}\left(\frac{p_e}{p_0} - 1\right)}{7.00098\sqrt{\left(\frac{p_e}{P_3}\right)^{1.42855}\left[1 - \left(\frac{p_e}{P_3}\right)^{0.28571}\right]\left[1 - \left(\frac{p_0}{P_3}\right)^{0.28571}\right]}} \tag{C2}$$

If p_e/p_0 is reduced far enough to choke the exit, the pressure ratio of the stream at the exit plane reaches a constant value of 0.5283 and the gross thrust efficiency becomes independent of the pressure surrounding the exit plane. Equation (C2) thus reduces to

$$\eta_{GA} = \frac{1.2680 - \frac{p_0}{P_3}}{1.81188\left[1 - \left(\frac{p_0}{P_3}\right)^{0.28571}\right]^{1/2}} \tag{C3}$$

The analytical gross thrust efficiencies for low pressure ratio nozzles are presented in figure 25 as a function of p_e/p_0, for several values of P_3/p_0. In the RESULTS AND DISCUSSION section (see also figs. 11 and 23) nozzle gross thrust efficiencies greater than 1.000 were calculated at Mach 0.6. At Mach 0.6 the external flow field around the nacelle resulted in a value for p_e/p_0 of about 1.04 with a value for P_3/p_0 of about 1.5. Analytical gross thrust efficiency could have been as high as 1.0005 (see fig. 25).

APPENDIX D

PRESSURE DISTRIBUTIONS

Pressure coefficients on the fan cowl from the inlet throat to the maximum nacelle diameter are plotted in figure 26 as a function of projected area ratio. The data were selected at the nominal mass flow ratio schedule (fig. 10). The Mach numbers corresponding to the minimum pressure coefficients are indicated as well as the Mach number at the start of the maximum diameter cylindrical section of the fan cowl.

Pressure coefficients on the fan boattail are plotted against projected area ratio in figure 27. At each Mach number the level of the last pressure coefficient on the fan cowl is shown for reference. This pressure was measured about 1.01 nacelle diameters upstream of the boattail juncture.

Pressure coefficient profiles are shown in figure 28 for the core boattail, in figure 29 for the scrubbed pylon, and in figure 30 for the external pylon.

Pressure profiles at the entrance to the fan nozzle are shown in figure 31 over a range of free stream Mach numbers and fan pressure ratios. The pressures are normalized to p_0 so that the ratio represents a local nozzle pressure ratio.

REFERENCES

1. Mort, Kenneth L.: Conference on V/STOL and STOL Aircraft. NASA SP-116, 1966.
2. Kutney, J.T.: Propulsion System Development for V/STOL Transports. Jour. Aircraft, vol. 3, no. 6, Nov.-Dec., 1966, pp. 489-497.
3. Rosen, George: Prop-Fan-A High Thrust, Low Noise Propulsor Paper 710470, SAE, May 1971.
4. Rulis, R.J.: Status of Current Development Activity Related to STOL Propulsion Noise Reduction. Presented at the National Air Transportation Meeting (Miami, Fla.), Apr. 24-26, 1973.
5. Wesoky, Howard: Low-Speed Wind-Tunnel Tests of a 50.8-Centimeter-(20-In.) Diameter 1.15-Pressure-Ratio Fan Engine Model. NASA TM X-3062, 1974.
6. Wesoky, H.L.; and Steffen, F.W.: Wind Tunnel Tests of a 20 Inch Diameter 1.15 Pressure Ratio Fan Engine Model. NASA TM X-71445, 1973.
7. Wasserbauer, Charles, A.: Calculated Performance Map of a $4\frac{1}{2}$-Stage 15.0-Centimeter - (5.9-In.) Mean-Diameter Turbine Designed for a Turbofan Simulator. NASA TM X-2822, 1973.
8. Baals, Donald D; Smith, Norman F.; and Wright, John B.: The Development and Application of High-Critical-Speed Nose Inlets. NACA Rep. 920, 1948.
9. Hancock, J.P.; and Hinson, B.L.: Inlet Development for the L-500. Paper 69-448, AIAA, Jane 1969.
10. Hetherington, R.: The Aerodynamics of Engine Component Design Problems Associated with Large Subsonic Aircraft. High Reynolds Number Subsonic Aerodynamics, AGARD-LS-37-70, Apr. 1969.
11. Bergman, Dave: Exhaust Nozzle Drag: Engine vs. Airplane Force Model. Paper 70-668, AIAA, June 1970.
12. Hoerner, Sighad F.: Fluid Dynamics Drag; Practical Information on Aerodynamic Drag and Hydrodynamic Resistance. 2nd edition, published by author, 1958.

TABLE I. - PYLON COORDINATES

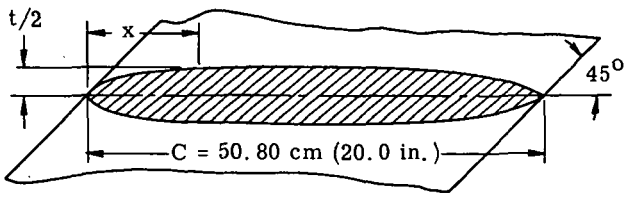

x/c	t/c	x/c	t/c
0	0	0.0750	0.0719
.0010	.0082	.0800	.0736
.0020	.0121	.0850	.0748
.0030	.0145	.0900	.0765
.0040	.0176	.0950	.0778
.0050	.0198	.1000	.0789
.0060	.0220	.1100	.0814
.0070	.0241	.1200	.0838
.0080	.0259	.1300	.0856
.0090	.0276	.1400	.0874
.0100	.0293	.1500	.0886
.0120	.0325	.1750	.0925
.0140	.0354	.2000	.0958
.0160	.0383	.2250	.0989
.0180	.0408	.2500	.1016
.0200	.0428	.3000	.1057
.0220	.0449	.3500	.1089
.0240	.0465	.4000	.1110
.0260	.0479	.4500	.1122
.0280	.0494	.5000	.1125
.0300	.0504	.5500	.1119
.0325	.0525	.6000	.1101
.0350	.0544	.6500	.1068
.0375	.0560	.7000	.1022
.0400	.0572	.7500	.0968
.0425	.0584	.7750	.0929
.0450	.0596	.8000	.0883
.0475	.0607	.8250	.0823
.0500	.0616	.8500	.0748
.0525	.0630	.8750	.0664
.0550	.0641	.9000	.0565
.0575	.0652	.9250	.0448
.0600	.0664	.9500	.0315
.0650	.0686	.9750	.0165
.0700	.0706	1.0000	0

TABLE II. - ANALYTICAL INLET FLOW PARAMETERS FOR INLET 1-1

Pressure ratio		Nondimensional weight flow ratio,[a]	Additive drag coefficient,	Stagnation point radius ratio,
p_a/P_0	p_b/P_0	$\left(W_F\sqrt{\theta_2}/\delta_2\right)/\left(W\sqrt{\theta}/\delta\right)_{REF}$	$C_{D,ADD}$	R_{STAG}/R_1
Free stream Mach number, $M_0 = 0.60$				
0.8648	0.8657	52.444	0.1575	0.9568
.8532	.8557	54.065	.1474	.9585
.8405	.8448	55.748	.1371	.9603
.8270	.8333	57.428	.1273	.9621
.8135	.8217	59.021	.1179	.9636
.7992	.8095	60.604	.1088	.9652
.7664	.7815	63.956	.09033	.9685
.7493	.7669	65.537	.08190	.9699
.7300	.7504	67.231	.07421	.9715
.7105	.7337	68.823	.06684	.9729
.6881	.7145	70.545	.05914	.9744
.6653	.6947	72.165	.05228	.9771
.6404	.6729	73.804	.04577	.9771
.6131	.6488	75.469	.04005	.9785
.5847	.6231	77.034	.03487	.9797
.5528	.5935	78.634	.02987	.9809
.5162	.5583	80.282	.02494	.9822
.4732	.5141	81.991	.02012	.9835
.4230	.4538	86.643	.01602	.9848
Free stream Mach number, $M_0 = 0.70$				
0.7641	0.7745	64.815	0.1244	0.9643
.7456	.7585	66.499	.1148	.9658
.7259	.7413	68.188	.1055	.9673
.7046	.7227	69.886	.09671	.9688
.6815	.7025	71.597	.08818	.9702
.6564	.6803	73.328	.07994	.9717
.6303	.6570	74.961	.07239	.9730
.5996	.6292	76.746	.06442	.9745
.5669	.5987	78.444	.05719	.9759
.5294	.5625	80.189	.05023	.9771
.4875	.5191	81.865	.04437	.9784
.4357	.4572	83.621	.03849	.9797
Free stream Mach number, $M_0 = 0.75$				
0.8530	0.8502	55.043	0.2022	0.9531
.8398	.8386	56.781	.1909	.9549
.8258	.8265	58.507	.1800	.9566
.8110	.8134	60.224	.1694	.9583
.7953	.7997	61.934	.1591	.9598
0.7786	0.7852	63.641	0.1489	0.9614
.7599	.7689	65.441	.1386	.9631
.7409	.7523	67.154	.1286	.9646
.7203	.7343	68.874	.1188	.9661
.6982	.7149	70.604	.1092	.9676
.6754	.6947	72.236	.1007	.9690
.6492	.6713	73.999	.09184	.9704
.6200	.6451	75.792	.08321	.9719
.5892	.6166	77.496	.07520	.9733
.5542	.5835	79.241	.06731	.9746
.5158	.5451	80.912	.06001	.9759
.4696	.4945	82.650	.05292	.9771
Free stream Mach number, $M_0 = 0.80$				
0.7683	0.7750	64.813	0.1558	0.9614
.7500	.7589	66.508	.1458	.9629
.7303	.7416	68.208	.1359	.9644
.7091	.7230	69.916	.1260	.9659
.6861	.7027	71.638	.1162	.9673
.6611	.6804	73.377	.1069	.9688
.6351	.6569	75.023	.09841	.9701
.6062	.6304	76.693	.09009	.9714
.5738	.5999	78.398	.08185	.9728
.5365	.5637	80.150	.07360	.9741
.4949	.5202	81.834	.06601	.9755
.4434	.4582	23.597	.05826	.9768
Free stream Mach number, $M_0 = 0.85$				
0.7562	0.7629	66.109	0.1659	0.9614
.7364	.7455	67.853	.1553	.9629
.7151	.7267	69.606	.1447	.9644
.6919	.7062	71.373	.1342	.9659
.6666	.6836	73.157	.1238	.9674
.6403	.6597	74.851	.1145	.9688
.6110	.6329	76.569	.1054	.9701
.5781	.6019	78.323	.09634	.9715
.5402	.5651	80.124	.08735	.9729
.4976	.5207	81.860	.07889	.9742
.4475	.4597	82.551	.07085	.9755

[a] $\left(W\sqrt{\theta}/\delta\right)_{REF}$ = 0.4536 kg/sec = 1.000 lb/sec.

TABLE III. - ANALYTICAL INLET FLOW PARAMETERS FOR INLET 2-2

Pressure ratio		Nondimensional weight flow ratio,[a]	Pressure ratio		Nondimensional weight flow ratio,[a]
p_a/P_0	p_b/P_0	$\left(W_F\sqrt{\theta_2}/\delta_2\right)\Big/\left(W\sqrt{\theta}/\delta\right)_{REF}$	p_a/P_0	p_b/P_0	$\left(W_F\sqrt{\theta_2}/\delta_2\right)\Big/\left(W\sqrt{\theta}/\delta\right)_{REF}$
Free stream Mach number, $M_0 = 0.60$			Free stream Mach number, $M_0 = 0.75$		
0.7474	0.7656	62.231	0.6408	0.6635	70.553
.7179	.7398	64.795	.5951	.6204	73.167
.6869	.7125	67.177	.5409	.5661	75.716
.6506	.6802	69.678	.4694	.4803	78.334
.6100	.6432	72.097	Free stream Mach number, $M_0 = 0.80$		
.5620	.5973	74.557			
.5018	.5342	77.077	0.7221	0.7358	64.799
Free stream Mach number, $M_0 = 0.70$			.6894	.7064	67.341
			.6522	.6725	69.893
0.7201	0.7370	64.837	.6089	.6321	72.470
.6873	.7078	67.368	.5569	.5811	75.091
.6501	.6741	69.909	.4941	.5110	77.543
.6068	.6340	72.477	Free stream Mach number, $M_0 = 0.85$		
.5564	.5847	74.974			
.4920	.5138	77.529	0.7063	0.7203	66.121
Free stream Mach number, $M_0 = 0.75$			.6705	.6878	68.735
			.6292	.6496	71.369
0.7139	0.7297	65.405	.5816	.6038	73.933
.6798	.6991	67.972	.5224	.5421	76.544

[a] $\left(W\sqrt{\theta}/\delta\right)_{REF} = 0.4536$ kg/sec = 1.000 lb/sec.

TABLE IV. - ANALYTICAL INLET FLOW PARAMETERS FOR INLET 2-1

Pressure ratio		Nondimensional weight flow ratio,[a] $\left(W_F\sqrt{\theta_2}/\delta_2\right)/\left(W\sqrt{\theta}/\delta\right)_{REF}$
p_a/P_0	p_b/P_0	
Free stream Mach number, $M_0 = 0.60$		
0.7569	0.7808	62.311
.7285	.7576	64.781
.6967	.7317	67.266
.6620	.7033	69.659
.6219	.6707	72.078
.5741	.6319	74.541
.5143	.5833	77.068
.4328	.5172	79.552
Free stream Mach number, $M_0 = 0.70$		
0.7330	0.7569	64.756
.6998	.7294	67.381
.6631	.6991	69.924
.6202	.6639	72.498
.5703	.6229	74.999
.5065	.5704	77.564
.4131	.4941	80.096
Free stream Mach number, $M_0 = 0.75$		
0.7261	0.7495	65.480
.6924	.7215	68.052
Free stream Mach number, $M_0 = 0.75$		
0.6538	0.6896	70.644
.6100	.6533	73.155
.5564	.6091	75.710
.4856	.5507	78.339
Free stream Mach number, $M_0 = 0.80$		
0.7357	0.7563	64.760
.7036	.7295	67.298
.6671	.6992	69.851
.6245	.6639	72.433
.5731	.6213	75.064
.5112	.5701	77.519
.4180	.4935	80.063
Free stream Mach number, $M_0 = 0.85$		
0.7200	0.7420	66.149
.6847	.7125	68.770
.6446	.6791	71.360
.5969	.6395	73.986
.5384	.5909	76.611
.4593	.5254	79.196

[a] $\left(W\sqrt{\theta}/\delta\right)_{REF}$ = 0.4536 kg/sec = 1.000 lb/sec.

TABLE V. - CHARACTERISTIC LENGTHS AND WETTED AREAS

	Characteristic length, X, cm	Wetted area, cm^2
Fan cowl with inlet 1-1	78.207	13 323
External pylon	76.20	3 123
Dorsal	50.80	779
Scrubbed pylon	50.80	884
Core	114.30	2 677

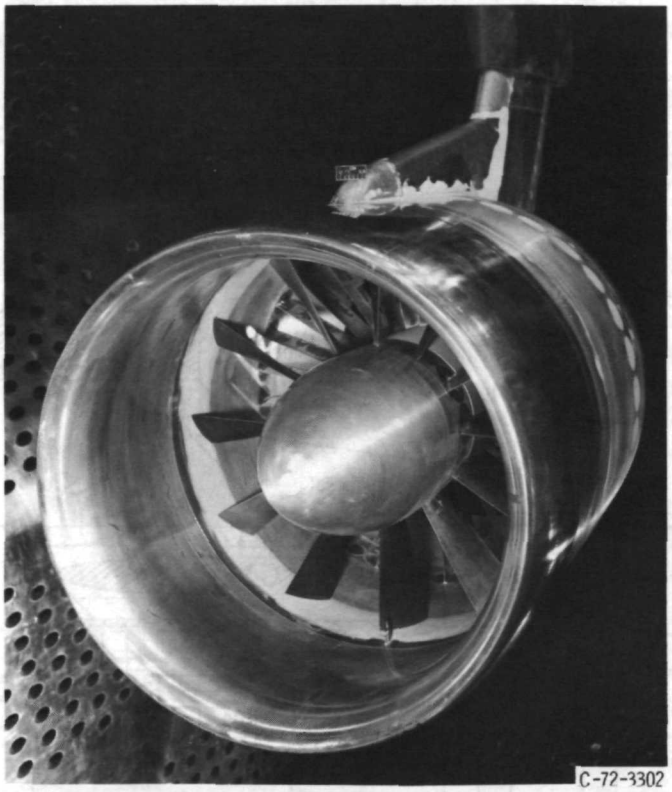

(a) Front view.

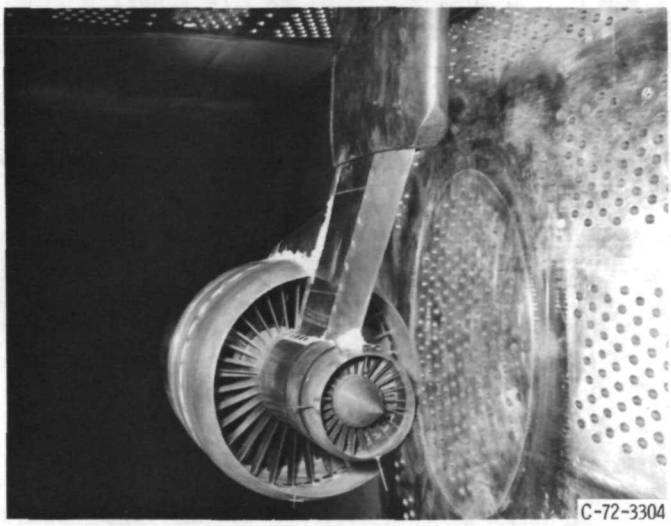

(b) Rear view.

Figure 1. - Nacelle in 8- by 6-Foot Supersonic Wind Tunnel.

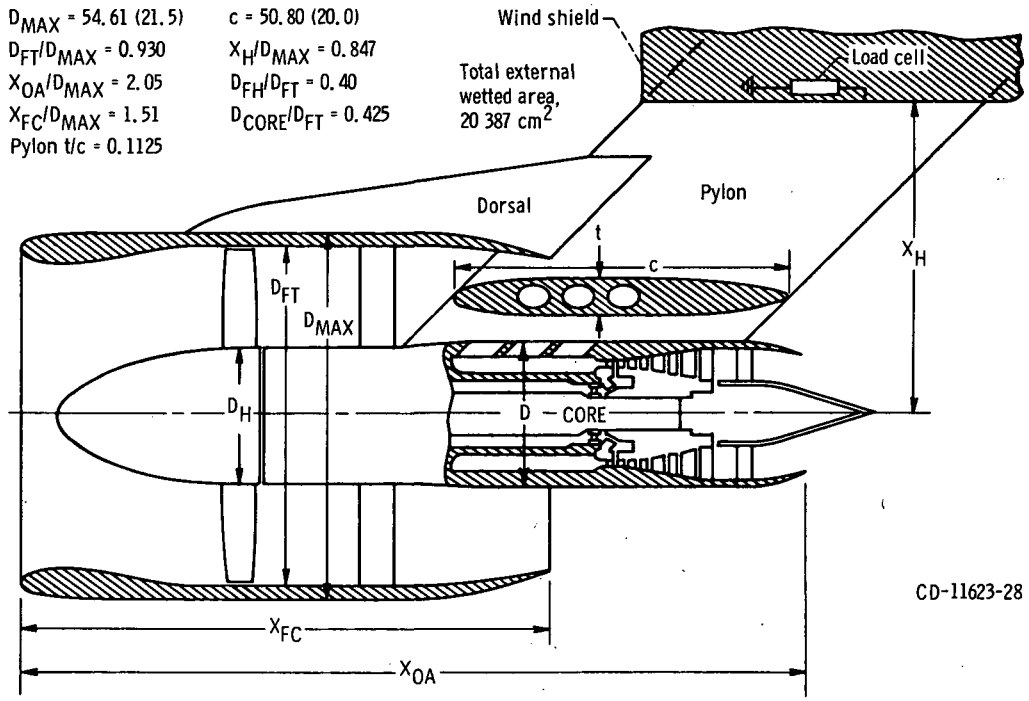

Figure 2. - Schematic of 1.15 fan pressure ratio nacelle. Dimensions are for nacelle with inlet 1-1. Dimensions are in centimeters (in.).

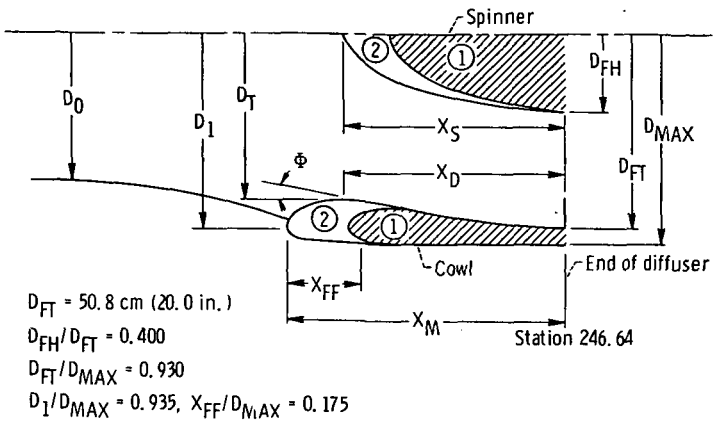

Spinner	X_S/D_{MAX}
1	0.414
2	.530

Inlet		A_1/A_T	A_1/A_{MIN}	X_D/D_{MAX}	X_M/D_{MAX}	Effective diffuser cone angle, σ, deg
Cowl	Spinner					
1	1	1.26	1.30	0.414	0.516	6.5
2	1	1.35	1.35	.530	.659	4.4
2	2	1.35	1.38	.530	.659	7.8

Figure 3. - Fan inlet geometry and dimensions. Spinner contour, NACA 1 series; external forebody contour, NACA 1 series; lip contour, 2:1 ellipse (long axis parallel to cowl axis); diffuser maximum turning angle, $\Phi = 10^0$. Stations are in centimeters.

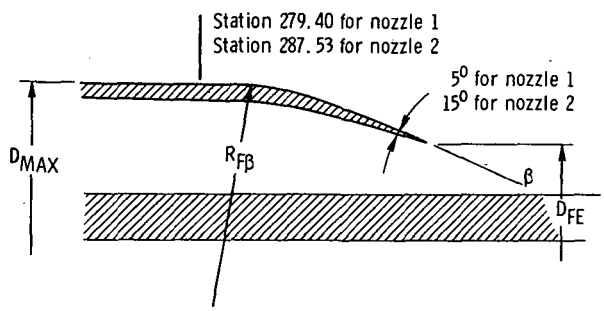

Nozzle	A_e, cm^2	β, deg	$R_{F\beta}/D_{MAX}$	D_{FE}/D_{MAX}	$A_{F\beta}/A_{MAX}$
1	1397	16	0.93	0.884	0.218
2	1593	15.3	.93	.934	.128

Figure 4. - Fan nozzle geometry details. Stations are in centimeters.

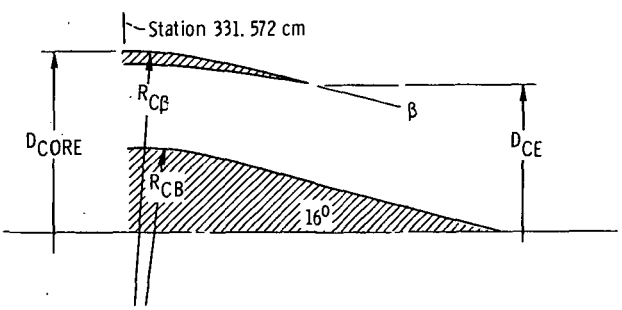

A_e, cm^2	β, deg	$\frac{R_{C\beta}}{D_{CORE}}$	$\frac{R_{CB}}{D_{CORE}}$	$\frac{D_{CE}}{D_{CORE}}$	$\frac{A_{C\beta}}{A_{MAX}}$
249	16	1.00	0.45	0.86	0.039

Figure 5. - Core nozzle geometry details.

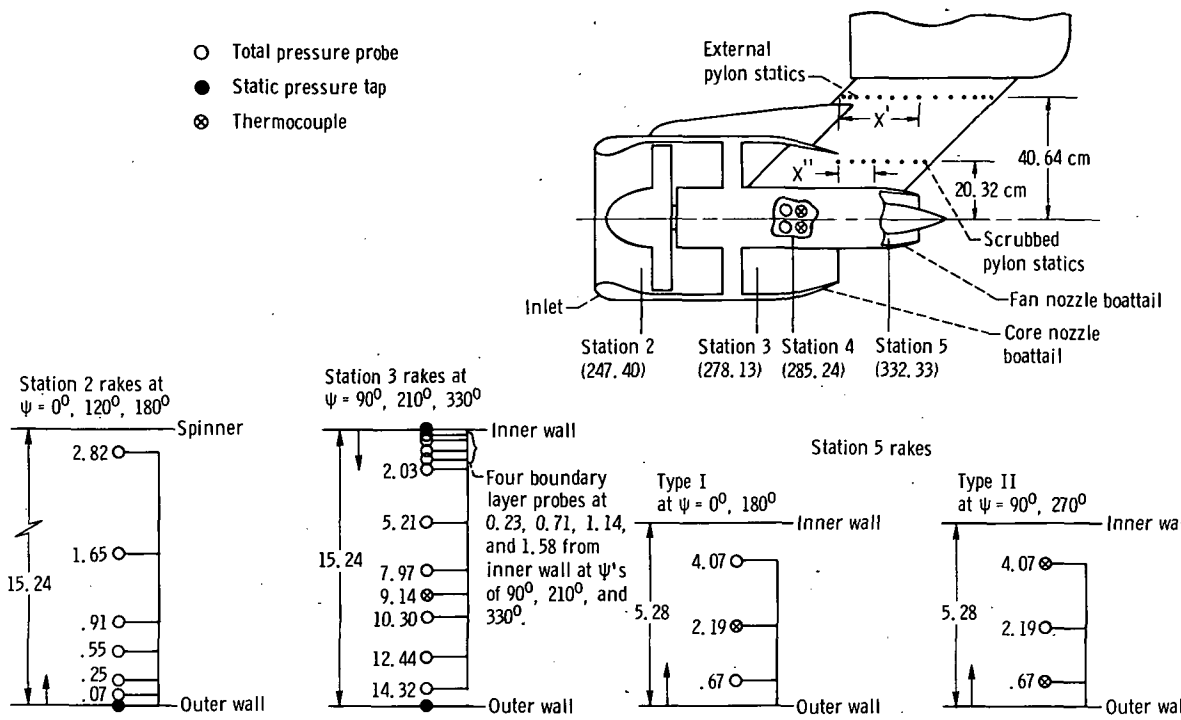

External inlet statics; axial distance from highlight						
0°	30°	90°	180°	210°	270°	300°
0.046	-----	-----	-----	0.046	0.046	-----
.092	-----	-----	-----	.092	-----	-----
.183	0.183	-----	-----	.183	.183	-----
.384	-----	-----	0.472	.384	-----	-----
.917	-----	0.917	-----	.917	.917	-----
1.836	-----	-----	-----	1.836	1.836	1.438
4.585	-----	-----	-----	4.585	2.870	-----
7.340	-----	-----	-----	7.340	-----	-----
9.170	-----	-----	-----	9.170	9.170	-----

Internal inlet statics; axial distance from highlight		
0	0	0.112
.221	.221	.312
.559	.559	.836
1.113	1.113	1.672
2.230	2.230	3.340
[a]4.460	[a]4.460	5.575
6.70	6.70	[a]7.831
10.10	10.10	12.34
14.63	14.63	16.89
19.15	19.15	21.40
23.65	23.65	25.90

[a]Used for weight flow calculation.

Fan nozzle boattail statics; axial distance from maximum nacelle diameter		
0°	210°	270°
5.56	5.56	5.56
9.73	9.73	9.73
12.58	12.58	12.58
14.90	14.90	14.90
17.30	17.30	17.30

Core nozzle boattail statics; axial distance from maximum core diameter		
0°	220°	270°
2.17	2.17	2.17
3.83	3.83	3.83
4.97	4.97	4.97
5.90	5.90	5.90
6.74	6.74	6.74
7.62	7.62	7.62

Pylon statics	
X'	X''
0	0
.254	10.16
.762	17.80
1.78	20.32
2.54	22.86
5.08	25.40
7.62	27.94
20.32	29.25
30.5	30.48
38.1	-----
40.6	-----
43.2	-----
45.8	-----
48.2	-----
49.6	-----
50.8	-----

Figure 6. - Simulator instrumentation. Linear dimensions and stations are given in centimeters. Angular coordinates (Ψ) measured counter-clockwise from bottom, looking aft.

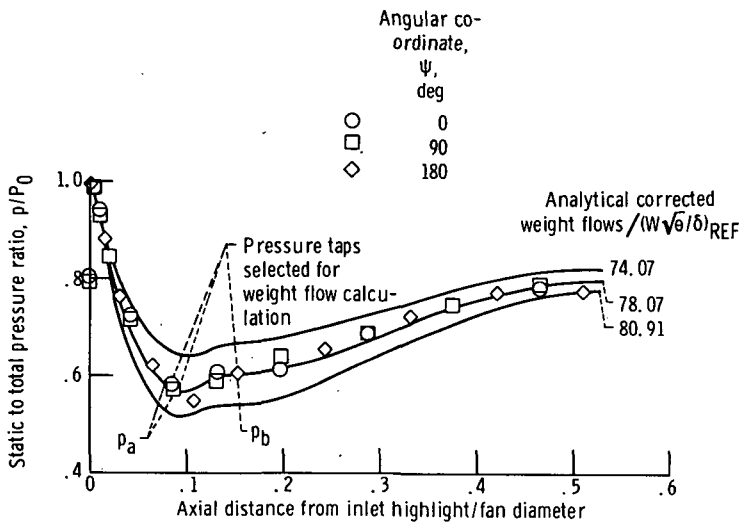

Figure 7. - Comparison of measured and calculated internal inlet pressures for inlet 1-1. Free stream Mach number, $M_0 = 0.75$.

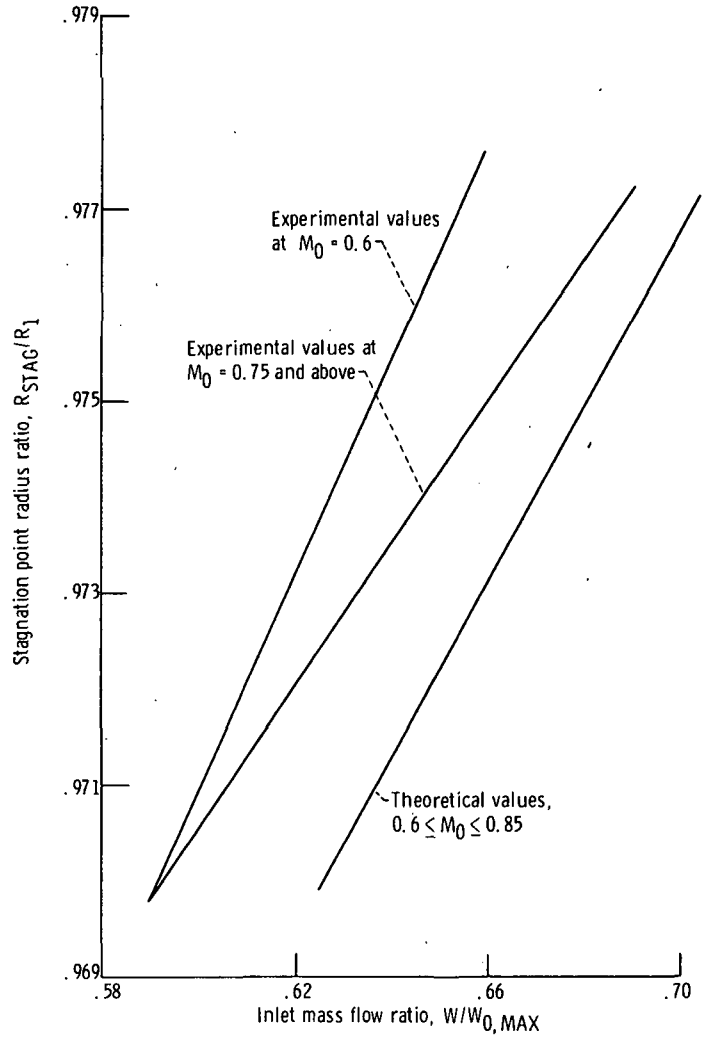

Figure 8. - Comparison of theoretical and experimental variation of stagnation point radial location with inlet mass flow ratio for inlet 1-1.

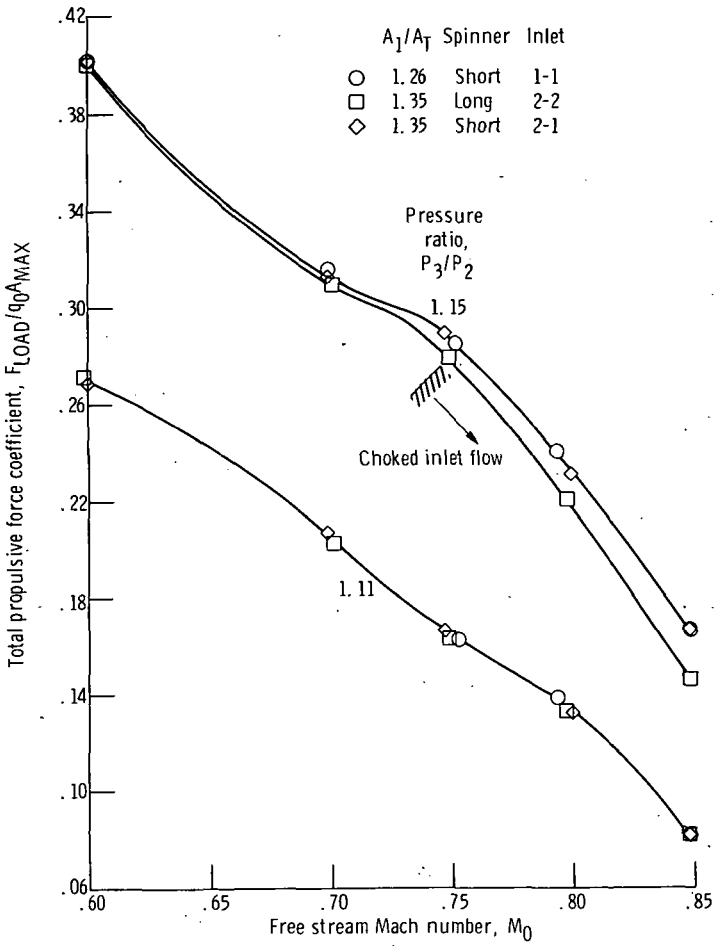

Figure 9. - Comparison of total propulsive force coefficients for three inlet configurations using nozzle 1.

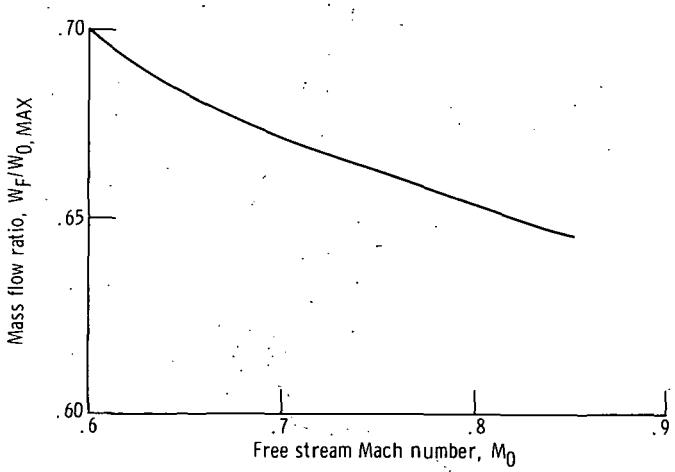

Figure 10. - Nominal mass flow ratio schedule. Fan nozzle 1; fan pressure ratio, 1.15.

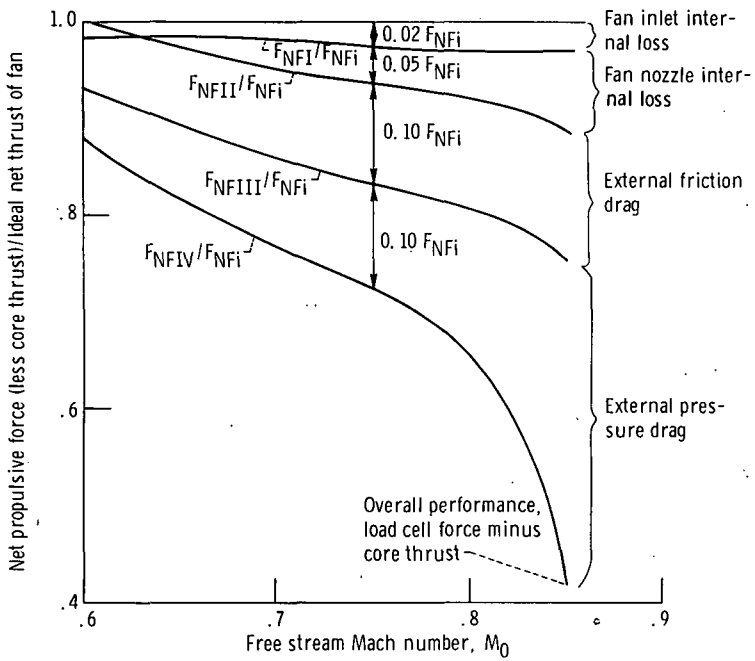

Figure 11. - Effect of cruise losses on net propulsive force of 1.15 fan pressure ratio propulsion system with inlet 1-1 and fan nozzle 1.

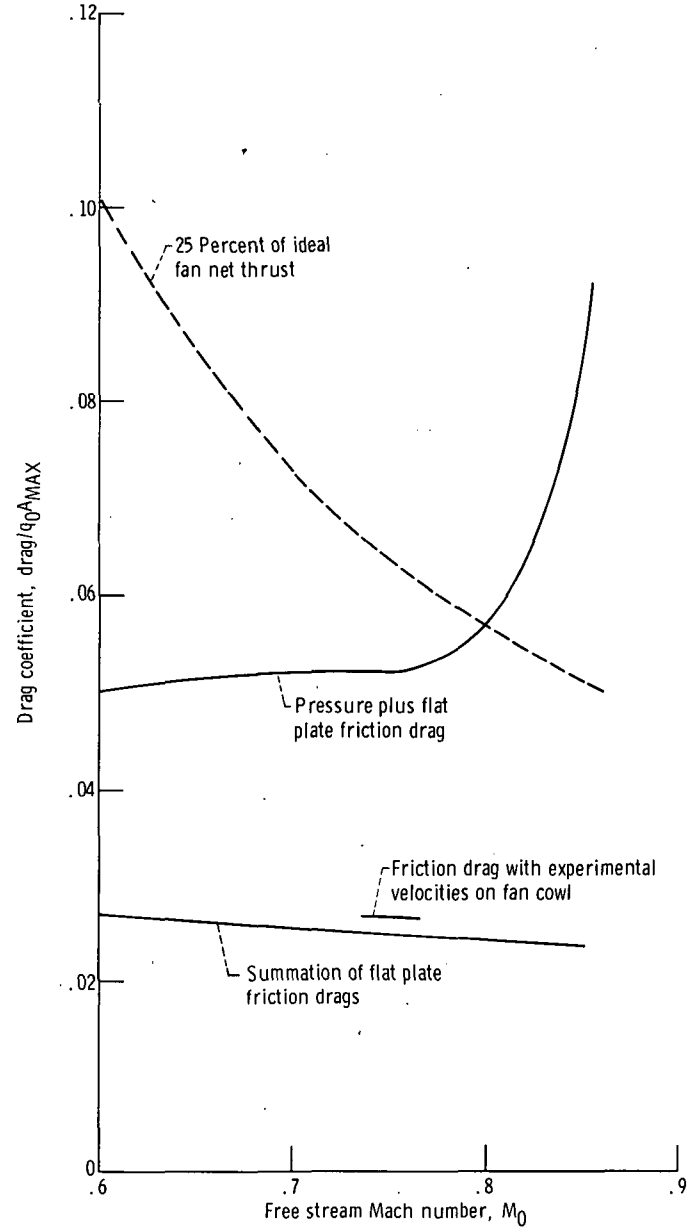

Figure 12. - Nacelle and pylon drag with inlet 1-1 and fan nozzle 1. Fan pressure ratio, 1.15.

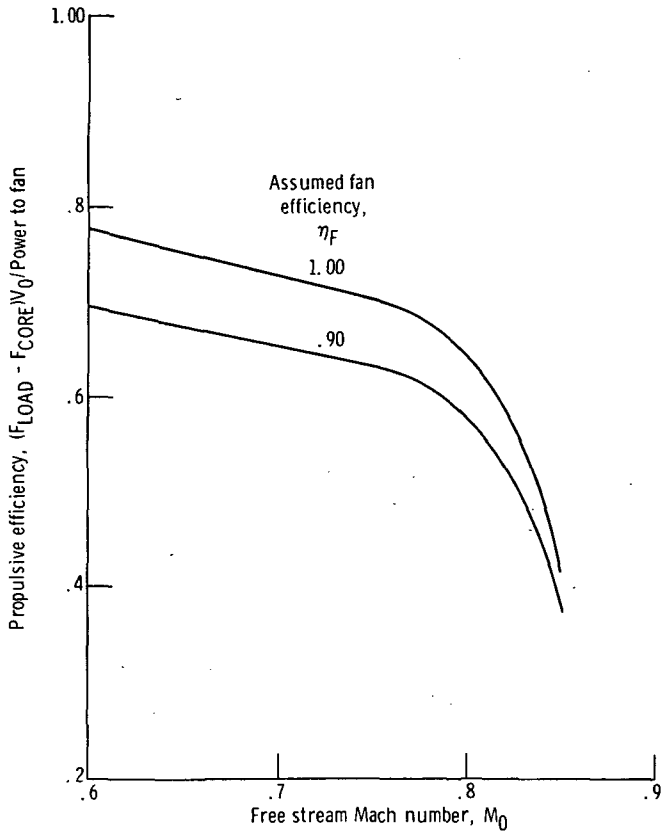

Figure 13. - Effect of cruise losses on propulsive efficiency of 1.15 pressure ratio turbofan propulsion system. Data obtained with inlet 1-1 and fan nozzle 1.

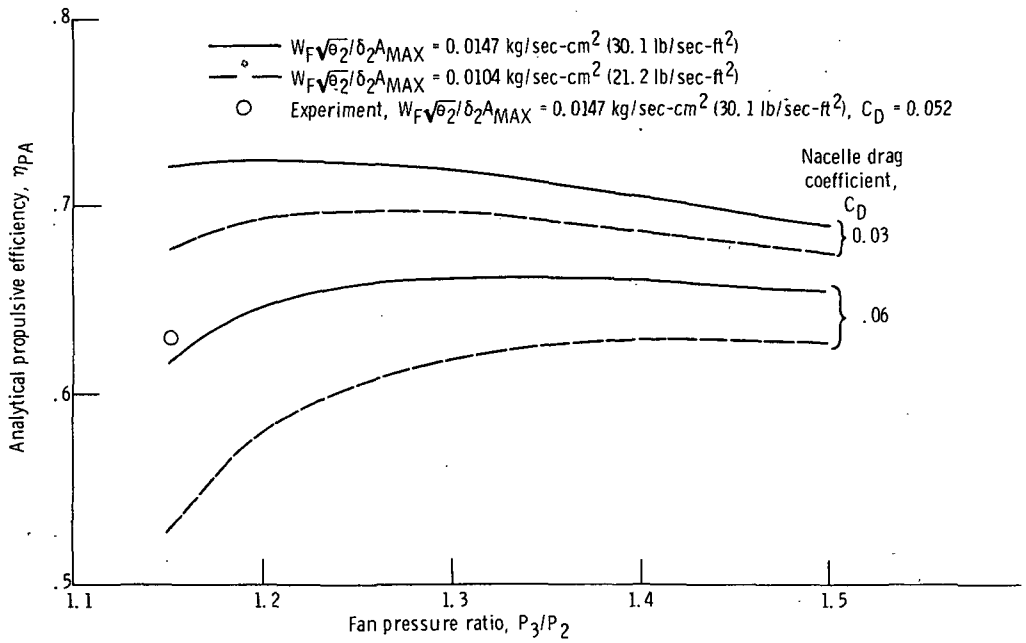

Figure 14. - Effects of fan pressure ratio on analytical propulsive efficiency for range of specific weight flows and drag coefficients. Free stream Mach number, M_0 = 0.75; assumed fan efficiency, η_F = 0.90.

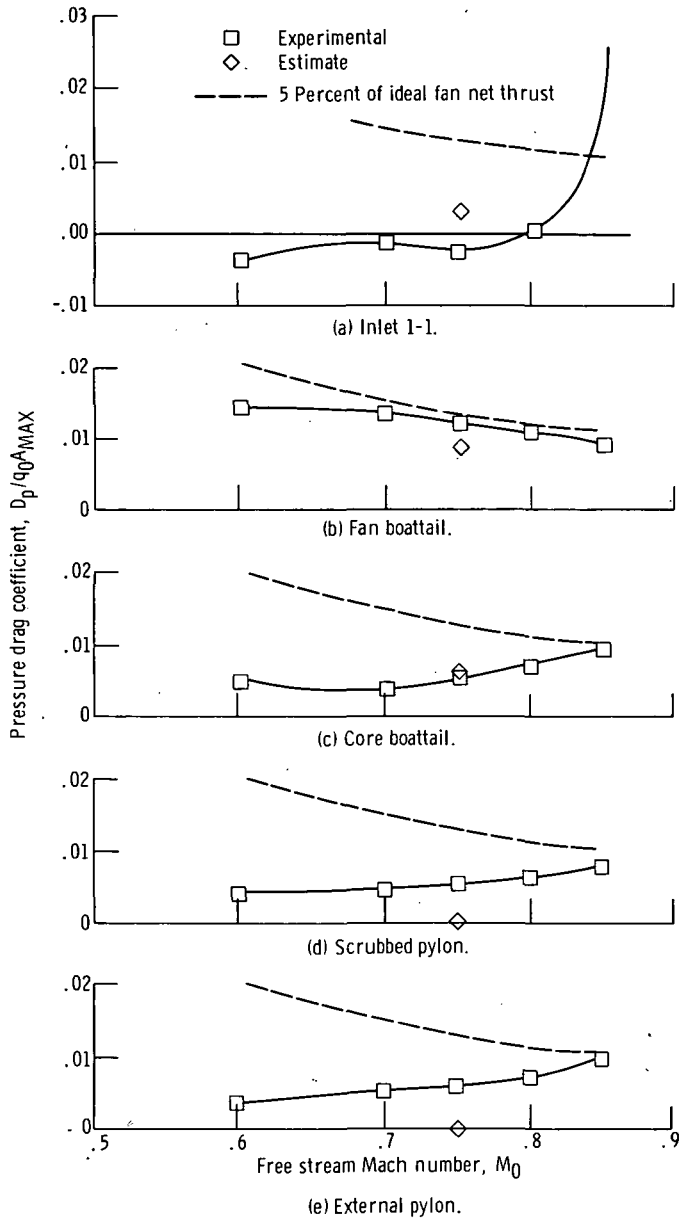

Figure 15. - Nacelle component pressure drags. Fan pressure ratio, 1.15.

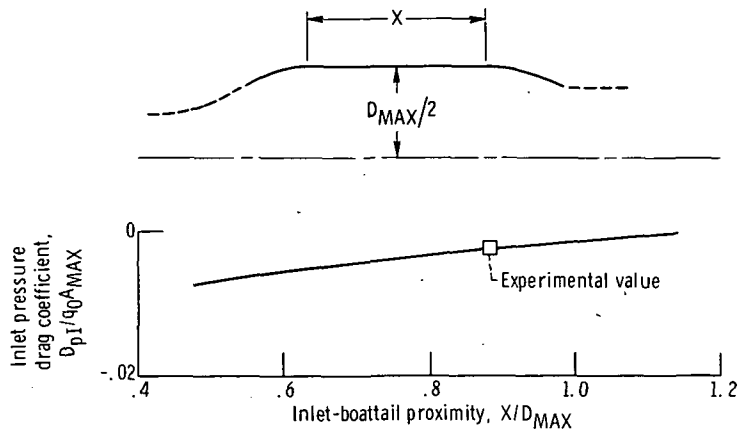

Figure 16. - Effect of boattail proximity on inlet pressure drag from potential flow analysis using inlet 1-1 and fan nozzle 1. Free stream Mach number, $M_0 = 0.75$; mass flow ratio, $W_F/W_{0,MAX} = 0.66$.

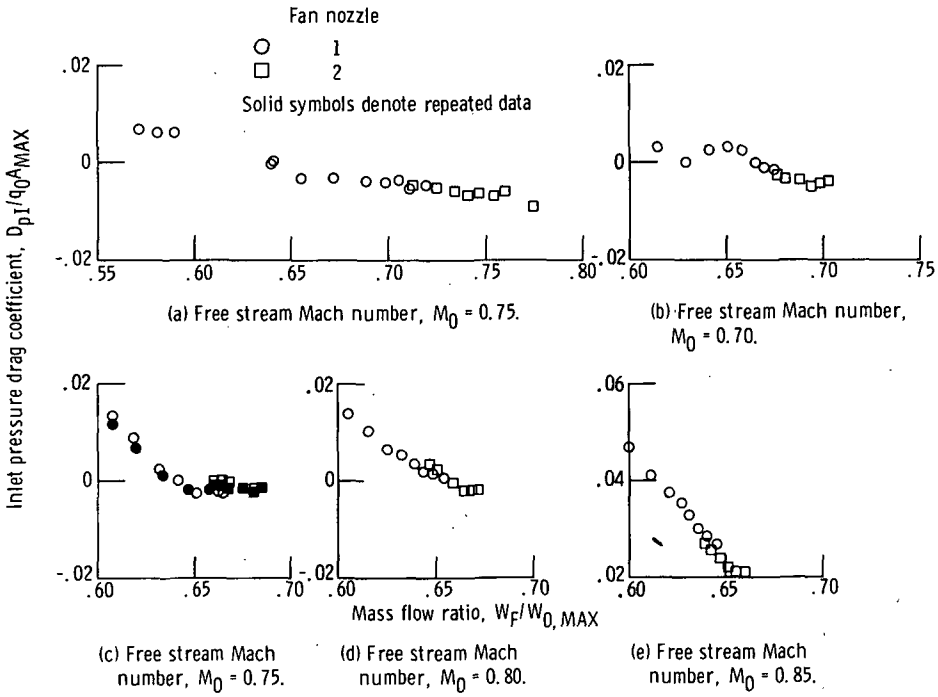

Figure 17. - Variation of inlet pressure drag with mass flow ratio for inlet 1-1.

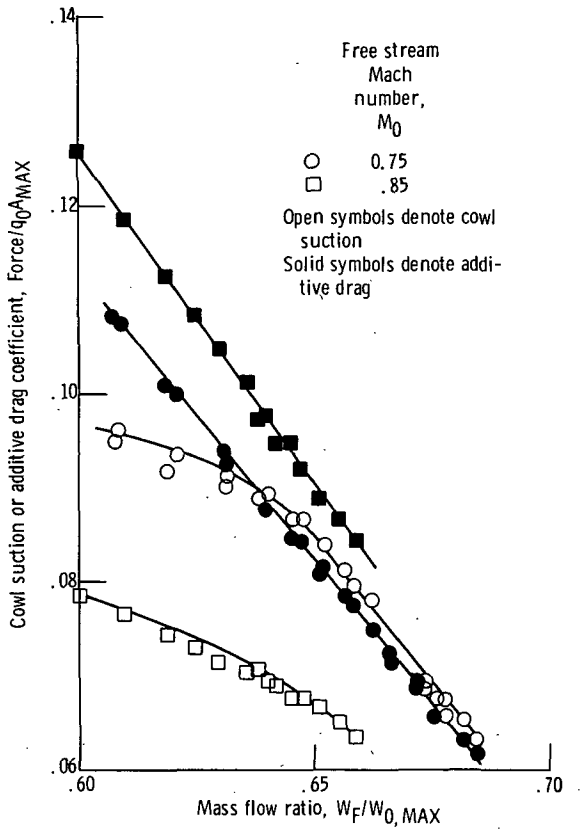

Figure 18. - Variation of cowl suction coefficient and additive drag coefficient with inlet mass flow ratio at free stream Mach numbers of 0.75 and 0.85 for inlet 1-1.

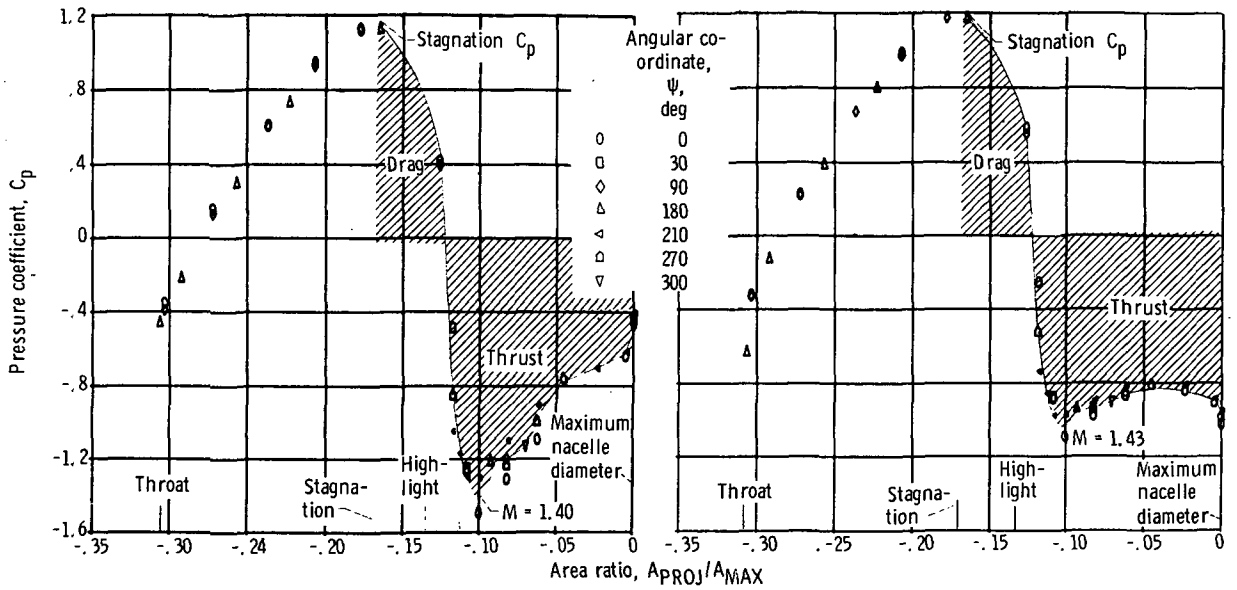

(a) Free stream Mach number, M_0 = 0.75; drag coefficient, C_{DPI} = -0.0020.

(b) Free stream Mach number, M_0 = 0.85; drag coefficient, C_{DPI} = 0.0208.

Figure 19. - Inlet pressure coefficient distributions at mass flow ratio of 0.658 for inlet 1-1.

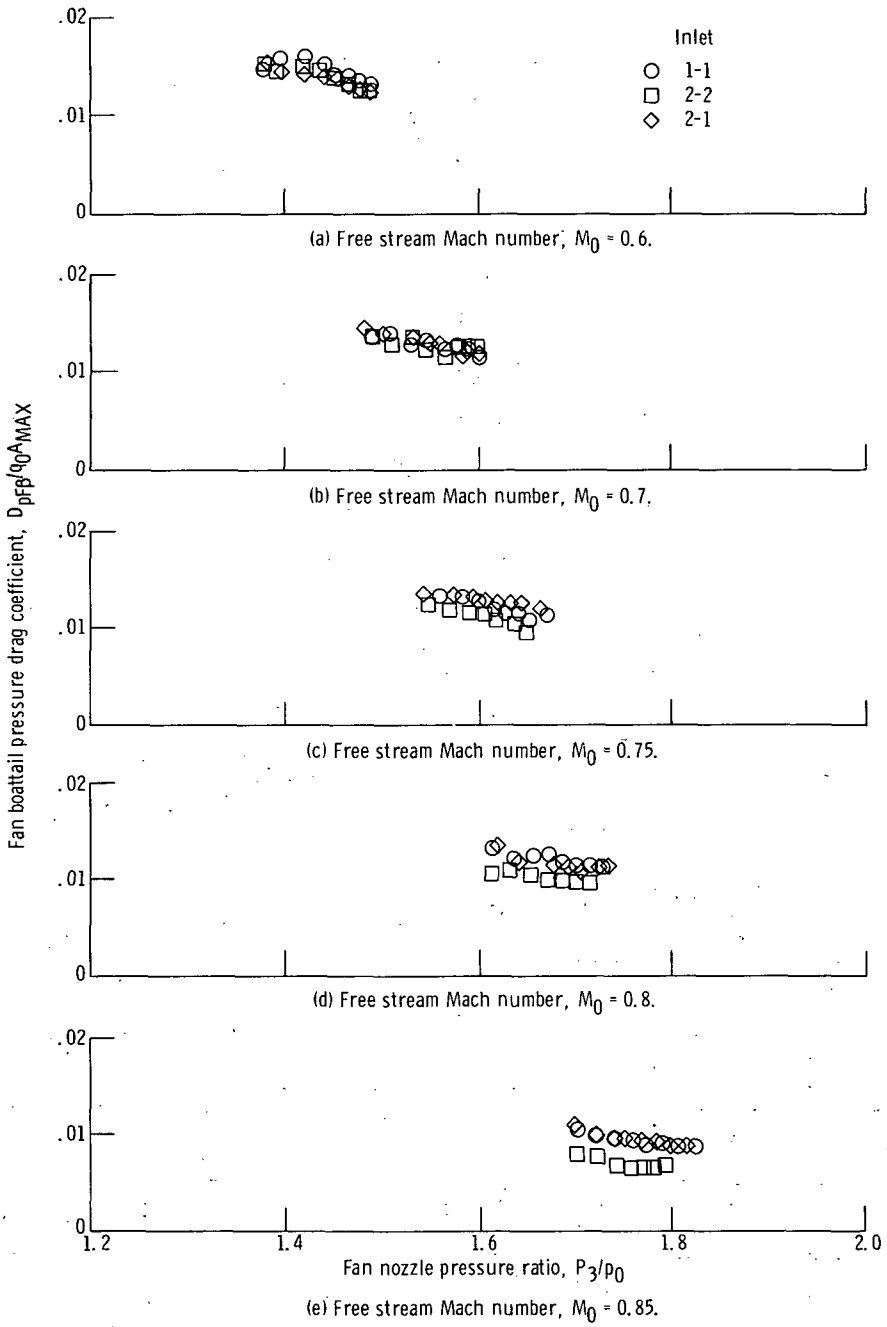

Figure 20. - Boattail pressure drag coefficients for fan nozzle 1 with various inlets.

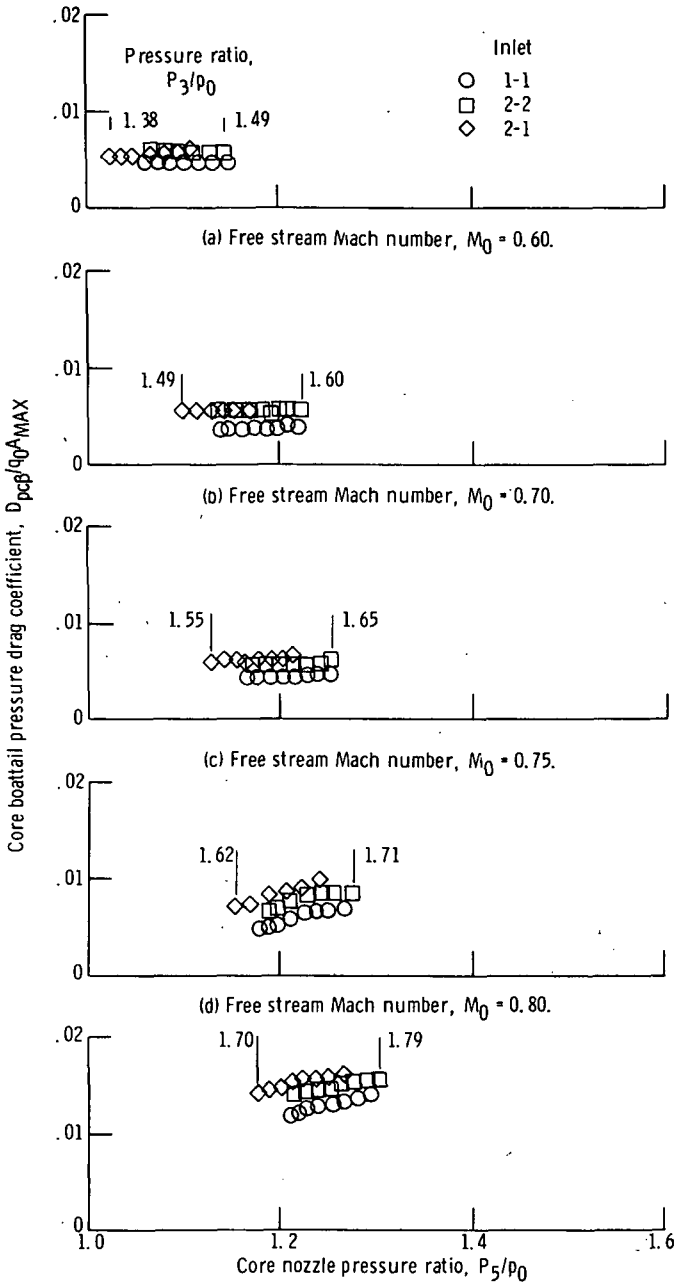

Figure 21. - Core boattail pressure drag coefficients with various inlets.

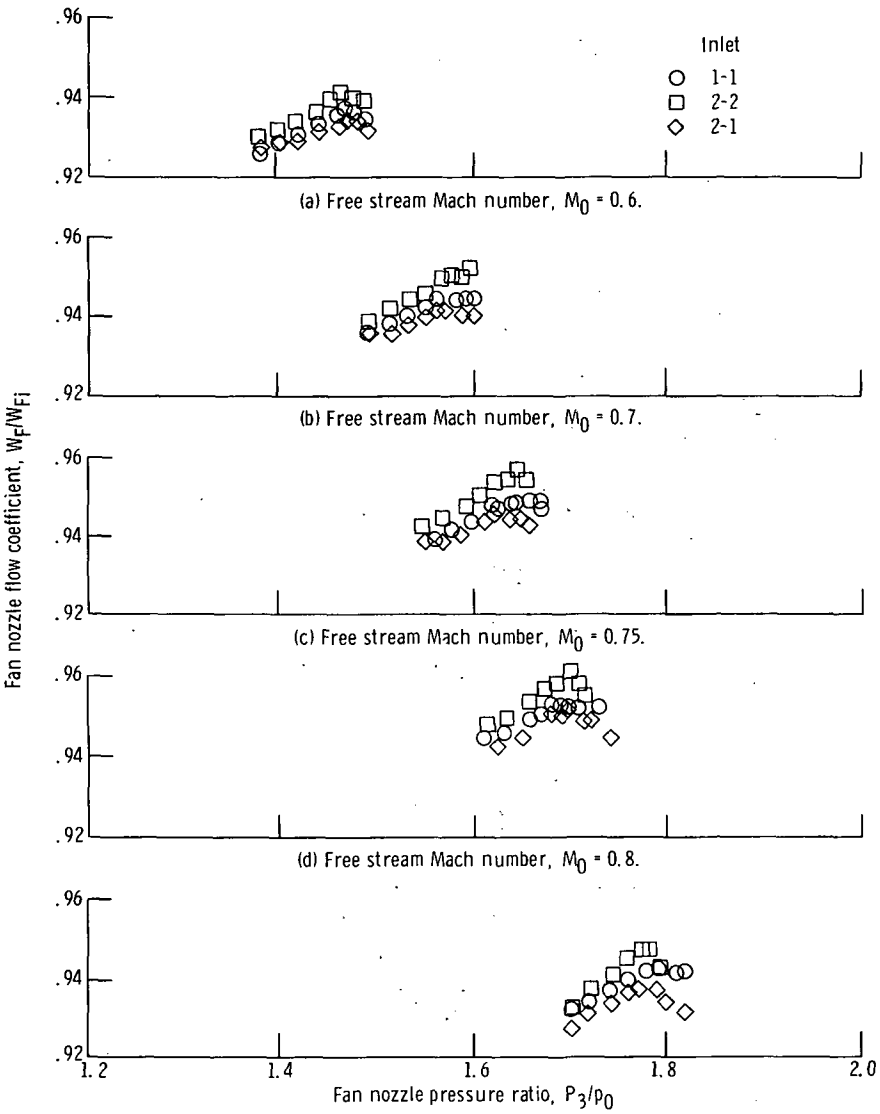

(a) Free stream Mach number, $M_0 = 0.6$.

(b) Free stream Mach number, $M_0 = 0.7$.

(c) Free stream Mach number, $M_0 = 0.75$.

(d) Free stream Mach number, $M_0 = 0.8$.

(e) Free stream Mach number, $M_0 = 0.85$.

Figure 22. - Flow coefficients for fan nozzle 1.

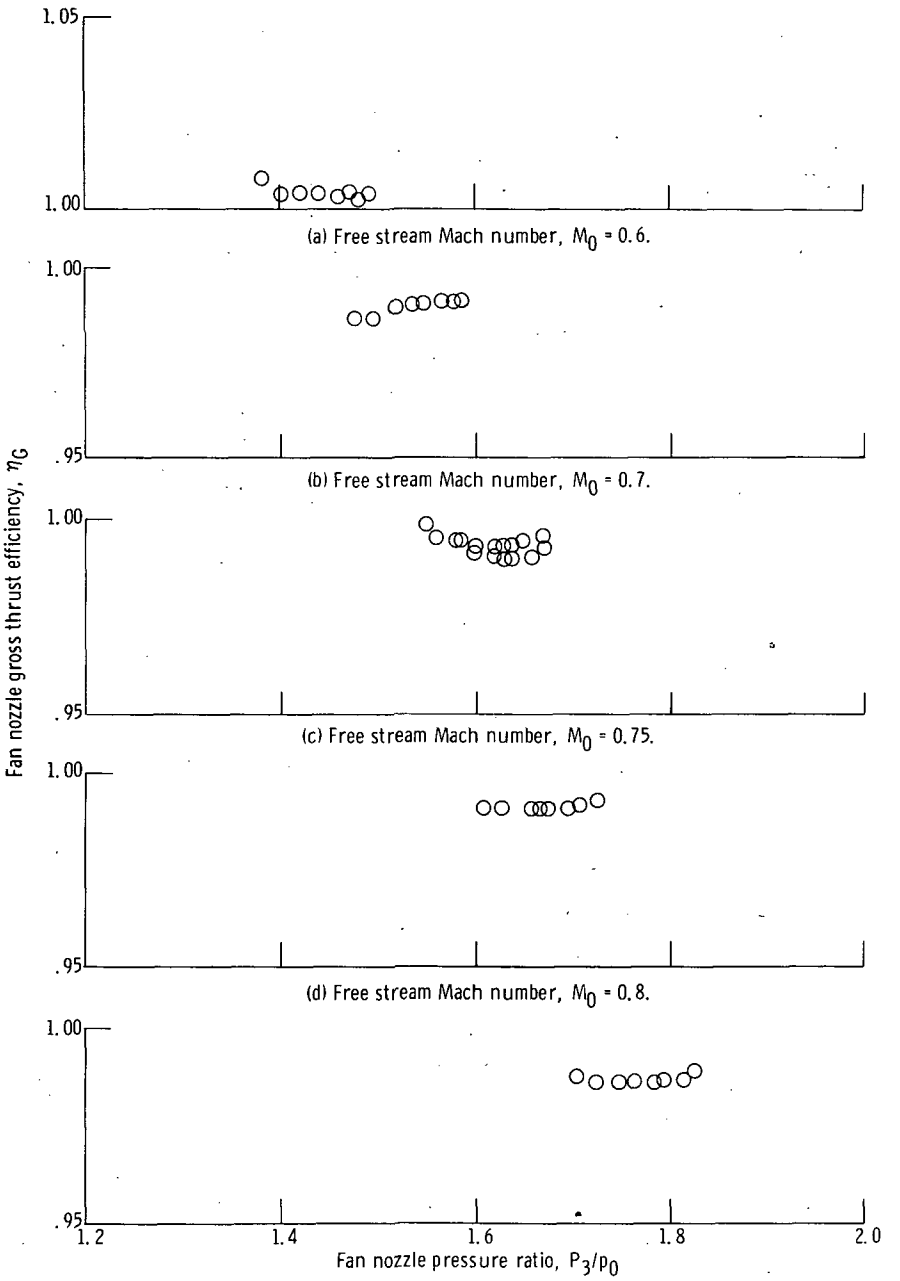

Figure 23. - Gross thrust coefficients for fan nozzle 1.

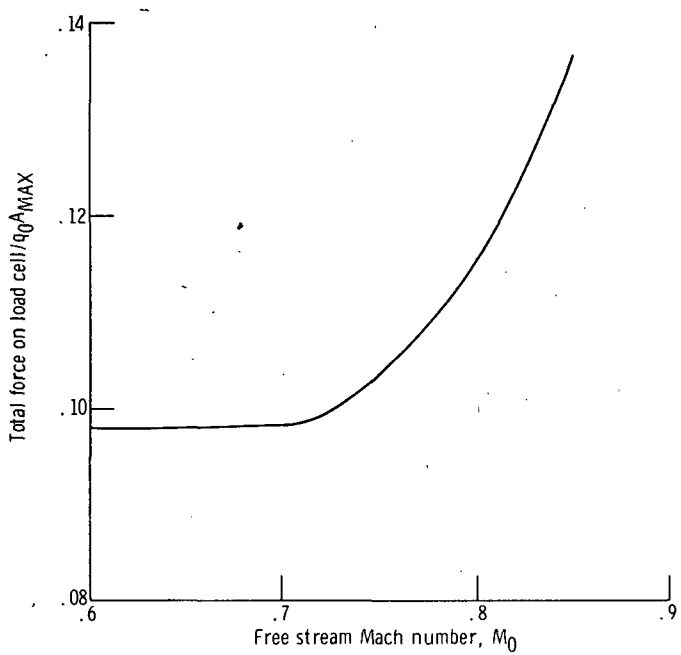

Figure 24. - Force on nacelle with feathered fan using inlet 1-1 and fan nozzle 2.

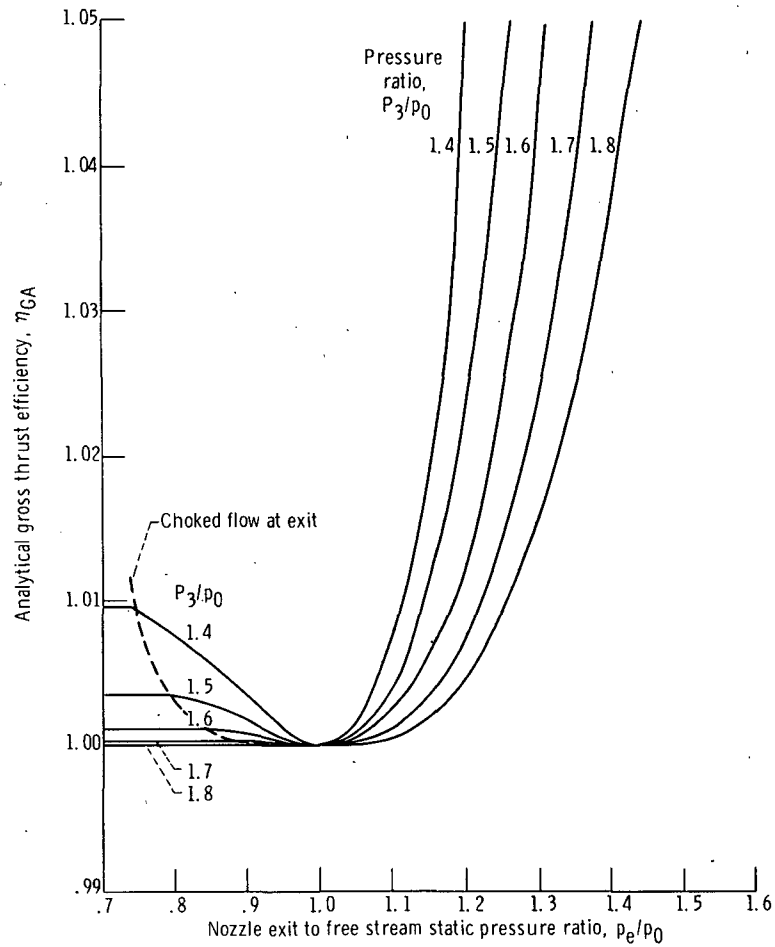

Figure 25. - Variation of analytical gross thrust efficiency with nozzle exit to free stream static pressure ratio. Air; specific heat ratio, $\gamma = 1.4$.

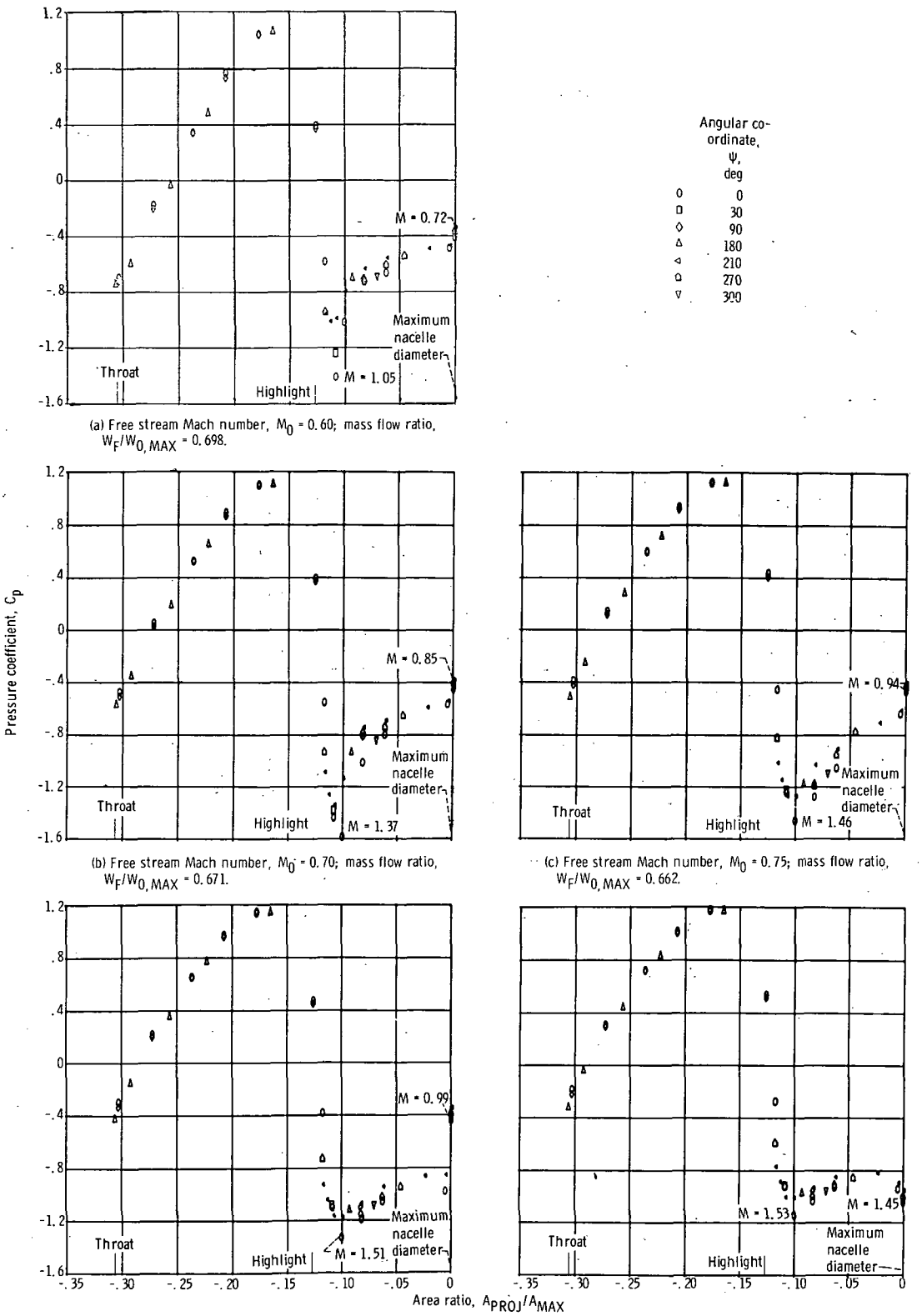

(a) Free stream Mach number, $M_0 = 0.60$; mass flow ratio, $W_F/W_{0,MAX} = 0.698$.

(b) Free stream Mach number, $M_0 = 0.70$; mass flow ratio, $W_F/W_{0,MAX} = 0.671$.

(c) Free stream Mach number, $M_0 = 0.75$; mass flow ratio, $W_F/W_{0,MAX} = 0.662$.

(d) Free stream Mach number, $M_0 = 0.79$; mass flow ratio, $W_F/W_{0,MAX} = 0.653$.

(e) Free stream Mach number, $M_0 = 0.85$; mass flow ratio, $W_F/W_{0,MAX} = 0.645$.

Figure 26. - Pressure coefficient profiles for inlet 1-1.

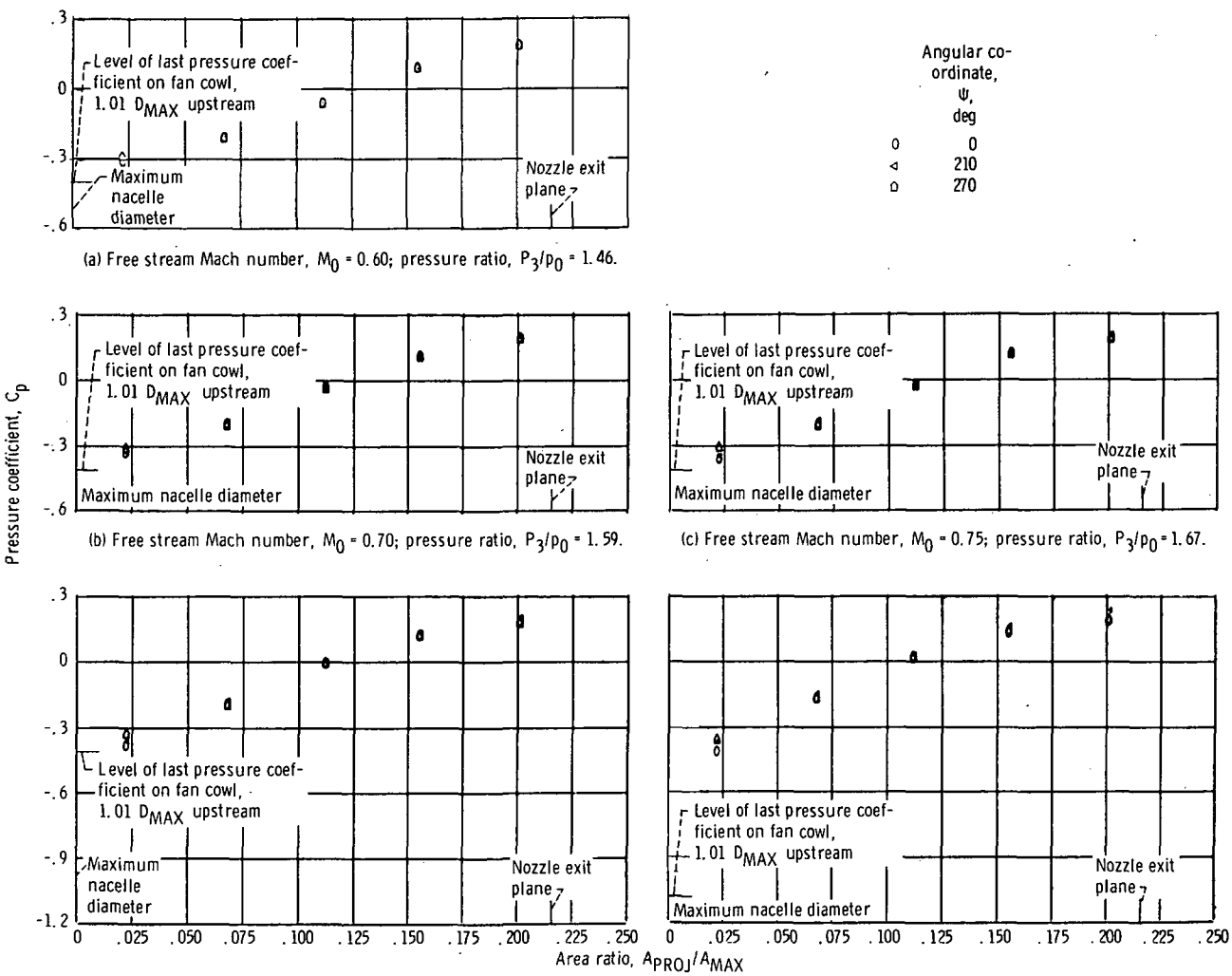

(a) Free stream Mach number, $M_0 = 0.60$; pressure ratio, $P_3/p_0 = 1.46$.

(b) Free stream Mach number, $M_0 = 0.70$; pressure ratio, $P_3/p_0 = 1.59$.

(c) Free stream Mach number, $M_0 = 0.75$; pressure ratio, $P_3/p_0 = 1.67$.

(d) Free stream Mach number, $M_0 = 0.79$; pressure ratio, $P_3/p_0 = 1.73$.

(e) Free stream Mach number, $M_0 = 0.85$; pressure ratio, $P_3/p_0 = 1.82$.

Figure 27. - Pressure coefficient for fan boattail 1 with inlet 1-1.

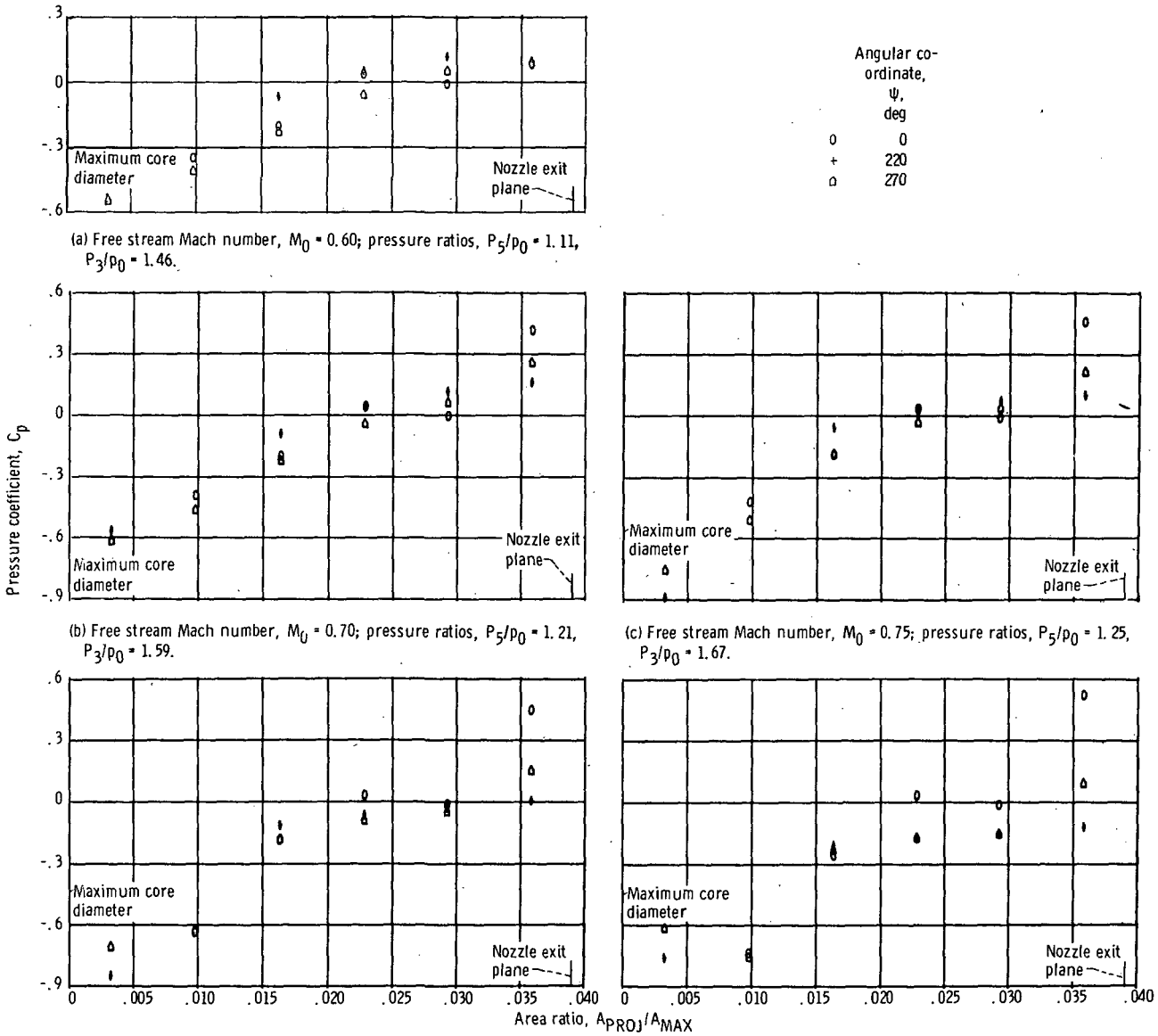

(a) Free stream Mach number, $M_0 = 0.60$; pressure ratios, $P_5/p_0 = 1.11$, $P_3/p_0 = 1.46$.

(b) Free stream Mach number, $M_0 = 0.70$; pressure ratios, $P_5/p_0 = 1.21$, $P_3/p_0 = 1.59$.

(c) Free stream Mach number, $M_0 = 0.75$; pressure ratios, $P_5/p_0 = 1.25$, $P_3/p_0 = 1.67$.

(d) Free stream Mach number, $M_0 = 0.79$; pressure ratios, $P_5/p_0 = 1.26$; $P_3/p_0 = 1.73$.

(e) Free stream Mach number, $M_0 = 0.85$; pressure ratios, $P_5/p_0 = 1.29$, $P_3/p_0 = 1.82$.

Figure 28. - Pressure coefficient profiles for core boattail with fan nozzle 1 and inlet 1-1.

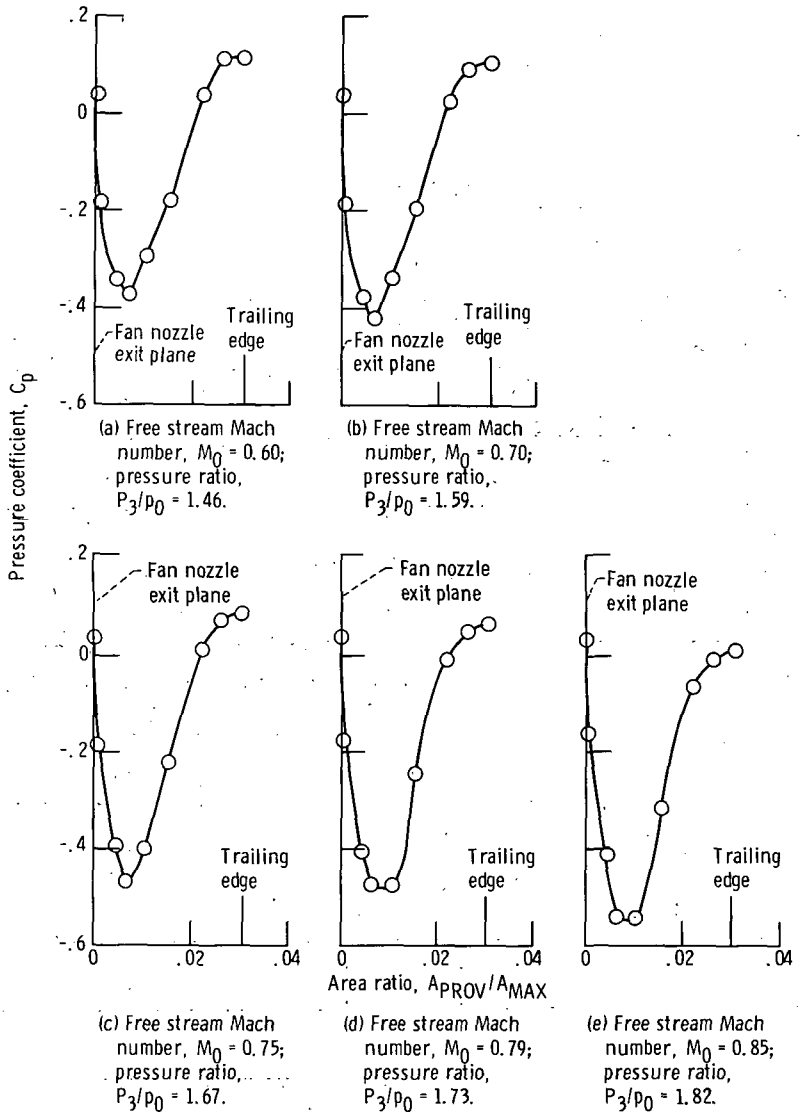

(a) Free stream Mach number, $M_0 = 0.60$; pressure ratio, $P_3/p_0 = 1.46$.

(b) Free stream Mach number, $M_0 = 0.70$; pressure ratio, $P_3/p_0 = 1.59$.

(c) Free stream Mach number, $M_0 = 0.75$; pressure ratio, $P_3/p_0 = 1.67$.

(d) Free stream Mach number, $M_0 = 0.79$; pressure ratio, $P_3/p_0 = 1.73$.

(e) Free stream Mach number, $M_0 = 0.85$; pressure ratio, $P_3/p_0 = 1.82$.

Figure 29. - Pressure coefficient profiles for portion of pylon scrubbed by fan jet with fan nozzle 1

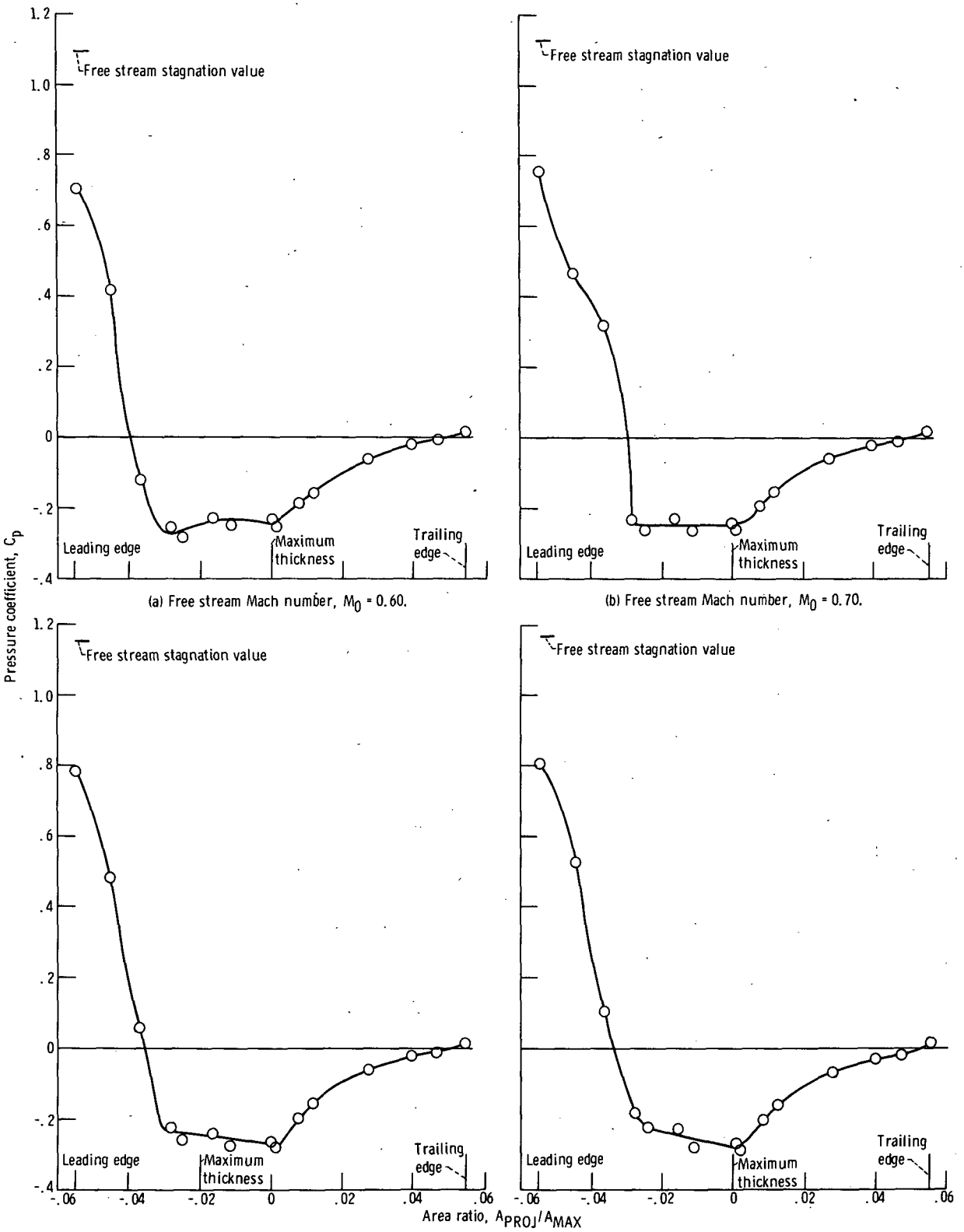

(a) Free stream Mach number, $M_0 = 0.60$.

(b) Free stream Mach number, $M_0 = 0.70$.

(c) Free stream Mach number, $M_0 = 0.75$.

(d) Free stream Mach number, $M_0 = 0.79$.

Figure 30. - Pressure coefficient profiles on external pylon.

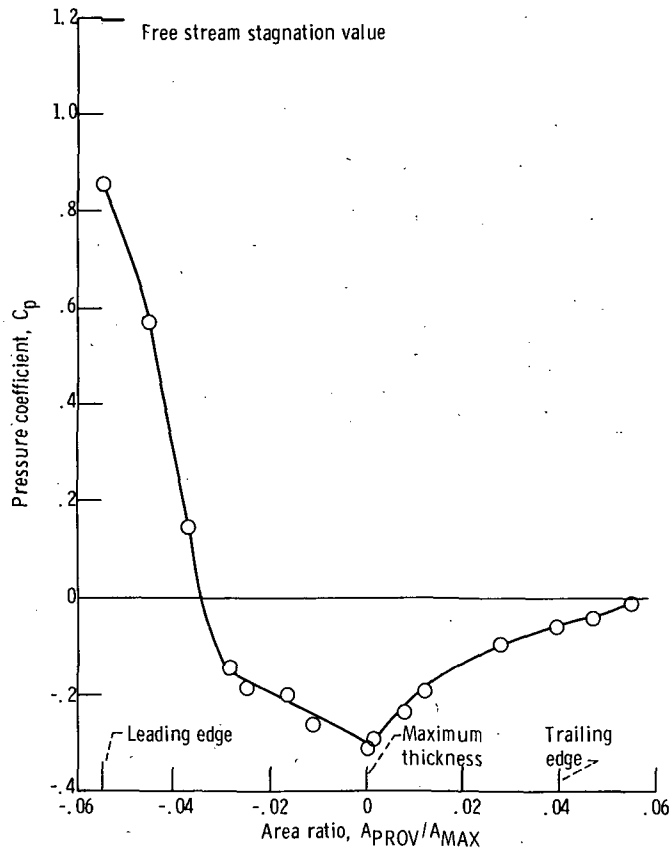

(e) Free stream Mach number, $M_0 = 0.85$.

Figure 30. - Concluded.

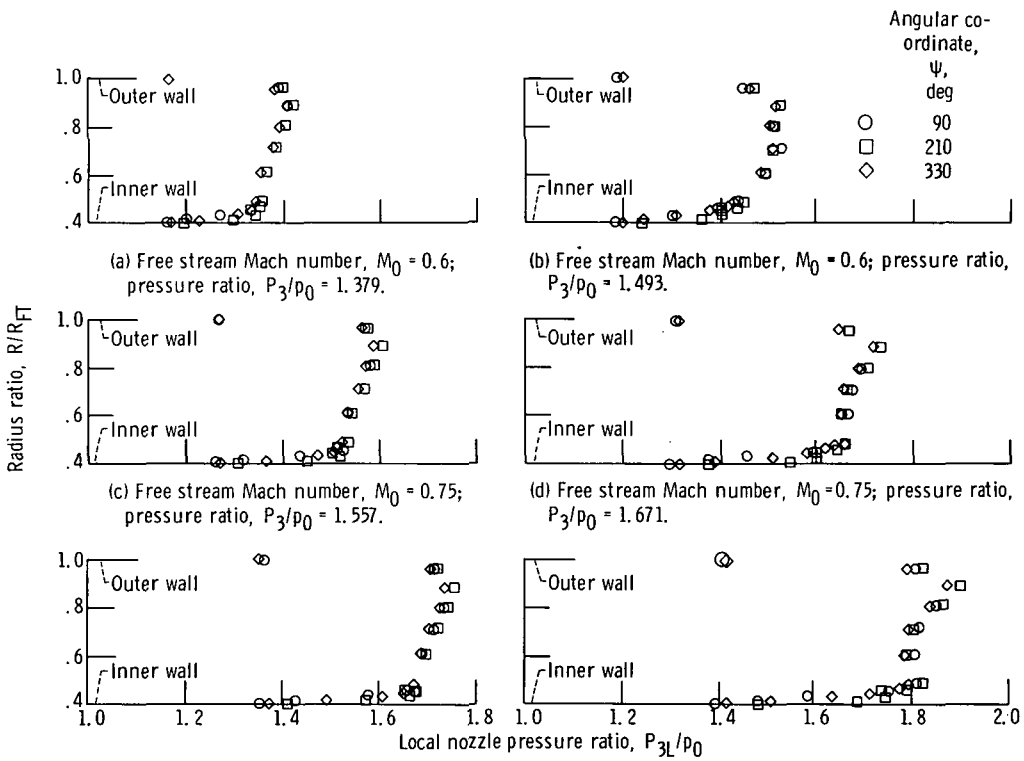

(a) Free stream Mach number, $M_0 = 0.6$; pressure ratio, $P_3/p_0 = 1.379$.

(b) Free stream Mach number, $M_0 = 0.6$; pressure ratio, $P_3/p_0 = 1.493$.

(c) Free stream Mach number, $M_0 = 0.75$; pressure ratio, $P_3/p_0 = 1.557$.

(d) Free stream Mach number, $M_0 = 0.75$; pressure ratio, $P_3/p_0 = 1.671$.

(e) Free stream Mach number, $M_0 = 0.85$; pressure ratio, $P_3/p_0 = 1.703$.

(f) Free stream Mach number, $M_0 = 0.85$; pressure ratio, $P_3/p_0 = 1.823$.

Figure 31. - Pressure profiles at entrance to fan nozzle with inlet 1-1.

Page Intentionally Left Blank

NATIONAL AERONAUTICS AND SPACE ADMINISTRATION
WASHINGTON, D.C. 20546

OFFICIAL BUSINESS
PENALTY FOR PRIVATE USE $300

SPECIAL FOURTH-CLASS RATE BOOK

POSTAGE AND FEES PAID
NATIONAL AERONAUTICS AND SPACE ADMINISTRATION
451

U.S.MAIL

POSTMASTER: If Undeliverable (Section 158 Postal Manual) Do Not Return

"The aeronautical and space activities of the United States shall be conducted so as to contribute . . . to the expansion of human knowledge of phenomena in the atmosphere and space. The Administration shall provide for the widest practicable and appropriate dissemination of information concerning its activities and the results thereof."

—NATIONAL AERONAUTICS AND SPACE ACT OF 1958

NASA SCIENTIFIC AND TECHNICAL PUBLICATIONS

TECHNICAL REPORTS: Scientific and technical information considered important, complete, and a lasting contribution to existing knowledge.

TECHNICAL NOTES: Information less broad in scope but nevertheless of importance as a contribution to existing knowledge.

TECHNICAL MEMORANDUMS: Information receiving limited distribution because of preliminary data, security classification, or other reasons. Also includes conference proceedings with either limited or unlimited distribution.

CONTRACTOR REPORTS: Scientific and technical information generated under a NASA contract or grant and considered an important contribution to existing knowledge.

TECHNICAL TRANSLATIONS: Information published in a foreign language considered to merit NASA distribution in English.

SPECIAL PUBLICATIONS: Information derived from or of value to NASA activities. Publications include final reports of major projects, monographs, data compilations, handbooks, sourcebooks, and special bibliographies.

TECHNOLOGY UTILIZATION PUBLICATIONS: Information on technology used by NASA that may be of particular interest in commercial and other non-aerospace applications. Publications include Tech Briefs, Technology Utilization Reports and Technology Surveys.

Details on the availability of these publications may be obtained from:

SCIENTIFIC AND TECHNICAL INFORMATION OFFICE

NATIONAL AERONAUTICS AND SPACE ADMINISTRATION

Washington, D.C. 20546